5-2021

Cholesterol and Cholesterol Bilayer Domains Inhibit Binding of Alpha-Crystallin to the Membranes Made of the Major Phospholipids of Eye Lens Fiber Cell Plasma Membranes

Raju Timsina
Boise State University

Geraline Trossi-Torres
Boise State University

Matthew O'Dell
Boise State University

Nawal K. Khadka
Boise State University

Laxman Mainali
Boise State University

Publication Information

Timsina, Raju; Trossi-Torres, Geraline; O'Dell, Matthew; Khadka, Nawal K.; and Mainali, Laxman. (2021). "Cholesterol and Cholesterol Bilayer Domains Inhibit Binding of Alpha-Crystallin to the Membranes Made of the Major Phospholipids of Eye Lens Fiber Cell Plasma Membranes". *Experimental Eye Research, 206*, 108544. https://doi.org/10.1016/j.exer.2021.108544

Cholesterol and Cholesterol Bilayer Domains Inhibit Binding of Alpha-Crystallin to the Membranes Made of the Major Phospholipids of Eye Lens Fiber Cell Plasma Membranes

Raju Timsina
Department of Physics
Boise State University
Boise, ID

Geraline Trossi-Torres
Biomolecular Sciences Graduate Program
Boise State University
Boise, ID

Matthew O'Dell
Biomolecular Sciences Graduate Program
Boise State University
Boise, ID

Nawal K. Khadka
Department of Physics
Boise State University
Boise, ID

Laxman Mainali*
Department of Physics
Boise State University
Boise, ID

and

Biomolecular Sciences Graduate Program
Boise State University
Boise, ID
laxmanmainali@boisestate.edu

Abstract

The concentration of α-crystallin decreases in the eye lens cytoplasm, with a corresponding increase in membrane-bound α-crystallin during cataract formation. The eye lens's fiber cell plasma membrane consists of extremely high cholesterol (Chol) content, forming cholesterol bilayer domains (CBDs) within the membrane. The role of high Chol content in the lens membrane is unclear. Here, we applied the continuous-wave electron paramagnetic resonance spin-labeling method to probe the role of Chol and CBDs on α-crystallin binding to membranes made of four major phospholipids (PLs) of the eye lens, i.e., phosphatidylcholine (PC), sphingomyelin (SM), phosphatidylserine (PS), and phosphatidylethanolamine (PE). Small unilamellar vesicles (SUVs) of PC, SM*, and PS with 0, 23, 33, 50, and 60 mol% Chol and PE* with 0, 9, and 33 mol% Chol were prepared using the rapid solvent exchange method followed by probe-tip sonication. The 1 mol% CSL spin-labels used during SUVs preparation distribute uniformly within the Chol/PL membrane, enabling the investigation of Chol and CBDs' role on α-crystallin binding to the membrane. For PC, SM*, and PS membranes, the binding affinity (K_a) and the maximum percentage of membrane surface occupied (MMSO) by α-crystallin decreased with an increase in Chol concentration. The K_a and MMSO became zero at 50 mol% Chol for PC and 60 mol% Chol for SM* membranes, representing that complete inhibition of α-crystallin binding was possible before the formation of CBDs within the PC membrane but only after the formation of CBDs within the SM* membrane. The K_a and MMSO did not reach zero even at 60 mol% Chol in the PS membrane, representing CBDs at this Chol concentration were not sufficient for complete inhibition of α-crystallin binding to the PS membrane. Both the K_a and MMSO were zero at 0, 9, and 33 mol% Chol in the PE* membrane, representing no binding of α-crystallin to the PE* membrane with and without Chol. The mobility parameter profiles decreased with an increase in α-crystallin binding to the membranes; however, the decrease was

more pronounced for the membrane with lower Chol concentration. These results imply that the membranes become more immobilized near the headgroup regions with an increase in α-crystallin binding; however, the Chol antagonizes the capacity of α-crystallin to decrease the mobility near the headgroup regions of the membranes. The maximum splitting profiles remained the same with an increase in α-crystallin concentration, but there was an increase in the maximum splitting with an increase in the Chol concentration in the membranes. It implies that membrane order near the headgroup regions does not change with an increase in α-crystallin concentration but increases with an increase in Chol concentration in the membrane. Based on our data, we hypothesize that the Chol and CBDs decrease hydrophobicity (increase polarity) near the membrane surface, inhibiting the hydrophobic binding of α-crystallin to the membranes. Thus, our data suggest that Chol and CBDs play a positive physiological role by preventing α-crystallin binding to lens membranes and possibly protecting against cataract formation and progression.

Keywords: Cholesterol, cholesterol bilayer domains, α-crystallin, phospholipid membranes, binding affinity, mobility parameter, maximum splitting, EPR spin-labeling method.

1. Introduction

Three major components of the fiber cell plasma membrane of the eye lens are phospholipids (PLs), cholesterol (Chol), and intrinsic proteins (Bassnett et al., 2011; Borchman et al., 1989; Cooper, 2000). Chol content is extremely high in lens membranes than in other eukaryotic membranes (Subczynski et al., 2017a). The Chol/PL molar ratio in eye lens membrane of chicken, cow, human, and whale ranges from 1 to 10 (Borchman et al., 2017; Zelenka, 1984), with whales having the highest Chol/PL molar ratio of 10 (Borchman et al., 2017). In the human eye lens, Chol/PL molar ratio is as high as 1.8 in cortical membranes and 4.4 in the nuclear membranes (Li et al., 1987; Mainali et al., 2017; Truscott, 2000; Widomska and Subczynski, 2019). The Chol/PL molar ratio in the human lens membrane increases with age (Mainali et al., 2017; Truscott, 2000; Widomska and Subczynski, 2019). An increase in Chol concentration saturates the membrane forming the phospholipid cholesterol domain (PCD) (Mainali et al., 2017, 2015a, 2013, 2012a). With further increase in Chol concentration, pure cholesterol bilayer domains (CBDs) start to form within the PCD (Mainali et al., 2017, 2015a, 2013, 2012a). CBDs were detected in the model membranes (Mainali et al., 2020, 2012b, 2011; Raguz et al., 2011a, 2011b), lens lipid membranes (Mainali et al., 2017, 2015a, 2013, 2012a; Raguz et al., 2009) as well as in the intact cortical and nuclear membranes isolated from human donors of 40, 46, and 53 years old (Mainali et al., 2019). Moreover, CBDs' size in the human lens lipid membranes increased with the donors' age and was larger in the nuclear than in the cortical membranes, representing that the Chol content in the membranes determines the CBDs' size (Mainali et al., 2017). The Chol/PL molar ratio in other cell membranes does not exceed 1.0 (Emmelot, 1977). The role of extremely high Chol content in the lens membrane is unclear.

Chol has multiple effects on cell membranes, such as changes in the fluidity, thickness, compressibility, water penetration, and intrinsic curvature of the membrane (Li et al., 1987; Subczynski et al., 2017b). Chol also induces phase separation in multicomponent lipid mixtures, partitions different coexisting lipid phases, and changes the integral membrane proteins' conformation (Yang et al., 2016). Furthermore, Chol promotes cellular activities like exocytosis (Rituper et al., 2012), endocytosis (Yue and Xu, 2015), cell signaling (Incardona and Eaton, 2000; Stottmann et al., 2011), trafficking membrane proteins (Ikeda and Longnecker, 2007), and condensing PLs (Daly et al., 2011; Hung et al., 2007). Chol enriched regions of the lens membrane termed rafts, which form by the mixture of PLs (mainly sphingolipids) and ~33 mol% Chol (de Almeida et al., 2003; Veatch and Keller, 2003), could participate and control cell signaling and potocytosis (Brown and London, 2000; Rujoi et al., 2003). Chol is necessary for the activity of the membrane-associated proteins, such as Na^+-Ca^{2+} exchanger or Na^+ -K^+ ATPase (Vemuri and Philipson, 1989). Additionally, Chol moderates nuclear and cortical lens lipids' structural order (Borchman et al., 1996). Since the eye lens contains more gap junctions than any other tissue and Chol is recognized to be connected with gap junctions (Biswas et al., 2010, 2009; Biswas and Lo, 2007), the high Chol content may have a connection with the gap junction too. The high Chol content has been suggested to support fiber-to-fiber stability during visual accommodation (Biswas et al., 2010). It has also been reported that the high Chol content and CBDs are necessary to

maintain lens-membrane homeostasis (Subczynski et al., 2012). Along with these functions, Chol may play a significant role in protein binding with membranes. Previously, It was reported that Chol antagonizes the association of plasma proteins to the liposomes made of PLs containing saturated fatty acids (Sean C. Semple et al., 1996).

In the eye lens, the crystallins, i.e., α, β, and γ-crystallin, account for more than 90% of the lens proteins (Horwitz, 2003; Horwitz et al., 1999). The α-crystallin alone accounts for up to 40% of the lens proteins (Horwitz, 2003; Horwitz et al., 1999). It was reported that α- and β-, but not γ-, crystallin modulate the human lens membranes' headgroup mobility during aging (Zhu et al., 2010). Therefore, we think that both α- and β-crystallin can bind with the lens membranes. Moreover, it was found that α-crystallin has the strongest affinity towards lens membranes (Boyle and Takemoto, 1996; Cenedella and Fleschner, 1992; Chandrasekher and Cenedella, 1997; Cobb and Petrash, 2000; Grami et al., 2005; Tang et al., 1998) and PL vesicles (Borchman and Tang, 1996; Cobb and Petrash, 2002a; Ifeanyi and Takemoto, 1991; Tang et al., 1998). The primary binding sites of α-crystallin in the lens membranes are the intrinsic PLs (Borchman and Tang, 1996; Chandrasekher and Cenedella, 1997; Ifeanyi and Takemoto, 1991). With age, the level of α-crystallin association with the lens membranes increases significantly (Cenedella and Fleschner, 1992; Chandrasekher and Cenedella, 1995; Fu et al., 1984; Lampi et al., 1998; Ma et al., 1998; Spector, 1984; Srivastava et al., 1996), which eventually deteriorates its chaperone activity and contributes to cataract formation (Friedrich and Truscott, 2010; Truscott, 2005). A recent clinical study also reported that the concentration of α-crystallin decreases in the lens cytoplasm, with a corresponding increase in membrane-bound α-crystallin during cataract formation (Datiles et al., 2016). Since the eye lens membrane consists of exceedingly high Chol content, it is intriguing to probe the role of Chol on α-crystallin binding to the PL membranes. The advantage of using model membranes is that it helps investigate the influence of Chol on the binding of α-crystallin with the individual PL membranes.

The lens membranes consist of four major PLs, i.e., phosphatidylcholine (PC), sphingomyelin (SM), phosphatidylserine (PS), and phosphatidylethanolamine (PE). The PL composition of the lens membranes changes dramatically with age and cataract (Borchman, 2020; Borchman et al., 2017; Borchman and Yappert, 2010; Huang et al., 2005; Mainali et al., 2017; Paterson et al., 1997; Truscott, 2000; Yappert et al., 2003), among species (Borchman, 2020; Borchman et al., 2017; Deeley et al., 2008; Stimmelmayr and Borchman, 2018), and with a location in the lens (Borchman et al., 1989; Deeley et al., 2008; Mainali et al., 2017; Raguz et al., 2009; Yappert et al., 2003). Also, the Chol content in the lens membranes changes with age and cataract (Jacob et al., 2001; Widomska and Subczynski, 2019), among species (Borchman et al., 2017; Zelenka, 1984), and with a location in the lens (Li et al., 1987; Mainali et al., 2017; Truscott, 2000; Widomska and Subczynski, 2019). The Chol/PL molar ratio increases with age and decreases with cataract development (Jacob et al., 2001; Mainali et al., 2017, 2015a; Truscott, 2000; Widomska and Subczynski, 2019). It was suggested that changes in lipid composition with age might contribute to the binding of α-crystallin to the lens membranes, causing a cataract (Borchman, 2020). With a difference in PL composition as well as Chol content among species, differences in the cataract onset age have been observed. For example, with SM plus dihydrosphingomyelin (DHSM) dominant and Chol/PL molar ratio up to 4 (Deeley et al., 2008), humans develop cataracts at 60 years of age (Borchman et al., 2017; Stimmelmayr and Borchman, 2018). However, with DHSM dominant and Chol/PL molar ratio of 10 (Borchman et al., 2017), whales do not develop cataracts even at 200 years of age. Most likely, the high amount of DHSM resists lipid oxidation, and high Chol content prevents α-crystallin association with the lens membranes (Borchman and Tang, 1996; Ifeanyi and Takemoto, 1991; Tang and Borchman, 1998) in whales and protect them from cataract formation. Previously, we found that the Chol/PL molar ratio as well as CBDs' size on the cortical and nuclear lens-lipid membranes of 61 to 70 years old human donors were smaller in cataractous lenses in comparison to clear lenses (Mainali et al., 2015a). Moreover, we found that CBDs size increases with an increase in Chol content in the lens membranes (Mainali et al., 2017). It implies that the larger Chol/PL molar ratio and CBDs size likely prevents α-crystallin binding to the lens membranes and helps prevent cataract formation and progression. Based on these observations, we speculate that the Chol content and PL composition likely have a strong connection with the binding of α-crystallin to the lens membranes and cataract formation. To understand such a plausible connection fundamentally, a systematic study probing the role of Chol on the α-crystallin binding to the PL membranes is necessary.

The role of Chol on the α-crystallin binding to the PL membranes has not gained sufficient attention. Moreover, the results of the existing studies (Cobb and Petrash, 2002a; Tang et al., 1998) are conflicting. Cobb and Petrash et al. (2002a) used PC and SM membranes with and without 40 mol% Chol and reported no significant difference in α-crystallin binding to these membranes. Tang et al. (1998) used disteroyl-phosphatidylcholine (DSPC), SM, and egg-phosphatidylcholine (egg-PC) membranes with Chol/PL weight ratio up to 1.0 (~64 mol% Chol) and reported a significant decrease in α-crystallin binding to DSPC and SM membranes with Chol. However, they reported a slight increase in the binding capacity of α-crystallin to the egg-PC membrane with Chol. An important point to note is that these studies calculated binding capacity in terms of the amount of α-crystallin bound to fixed amounts of membranes with and without Chol. Moreover, at the 40 mol% Chol used by Cobb and Petrash et al. (2002a), CBDs do not form within the membranes. Surprisingly, there is no study probing the Chol and CBDs' role on α-crystallin binding to the PS and PE membranes. Therefore, a detailed study investigating the Chol and CBDs' role on α-crystallin binding to individual PL membranes made of all four major PLs of the eye lens (i.e., PC, SM, PS, and PE) is imperative.

We recently developed an EPR spin-labeling approach to investigate the binding of α-crystallin to the individual and two-component mixtures of four major PLs of the eye lens membranes, i.e., 1-palmitoyl-2-oleoyl-*sn*-glycero-3-phosphatidylcholine (POPC), SM,1-palmitoyl-2-oleoyl-*sn*-glycero-3-phosphatidylserine (POPS), and 1-palmitoyl-2-oleoyl-*sn*-glycero-3-phosphatidylethanolamine (POPE) (Mainali et al., 2021; Timsina et al., 2021). This study used the recently developed EPR method to investigate the Chol and CBDs' role on α-crystallin binding to the POPC, SM*, POPS, and POPE* membranes, where * represents the presence of 20 mol% POPS. Small unilamellar vesicles (SUVs) were prepared using the rapid solvent exchange method (RSEM) followed by the probe-tip sonication. The RSEM preserves the compositional homogeneity throughout the membrane suspensions. CBDs start to form at 50, 48, 46, and 33 mol% Chol in the PC, SM, PS, and PE membranes, respectively (Mainali et al., 2020). The cholesterol analog cholestane spin-labels (CSL), in 1 mol%, were incorporated into the membranes to monitor the binding of α-crystallin to the membranes. The unique feature of the CSL spin-label is that it can uniformly distribute within Chol/PL membrane, making it possible to probe the role of Chol on α-crystallin binding to the membrane. Unlike in the previous studies probing the Chol's role on the α-crystallin binding to the PL membrane, the unique parameters we estimated are binding affinity (K_a) in terms of inverse micromole (μM^{-1}) of α-crystallin, the maximum percentage of membrane surface occupied (MMSO) by the α-crystallin, and the change in physical properties (maximum splitting and mobility parameter) of the membranes after α-crystallin binding. The mobility parameter gives the orientational and rotational dynamics of the spin-label in the membrane (Schreier et al., 1978). The maximum splitting parameter is related to the order parameter that gives the amplitude of the wobbling motion of the long axes of the spin-label in the membrane (Kusumi et al., 1986a; Mainali et al., 2012b; Raguz et al., 2011a). Our results help to understand the positive physiological role of Chol and CBDs in preventing α-crystallin binding with the lens membranes and possibly protecting against cataract formation and progression.

2. Materials and Methods

2.1. Materials

Lipids, 1-palmitoyl-2-oleoyl-*sn*-glycero-3-phosphatidylcholine (POPC), egg sphingomyelin (SM), 1-palmitoyl-2-oleoyl-*sn*-glycero-3-phosphatidylserine (POPS), 1-palmitoyl-2-oleoyl-*sn*-glycero-3-phosphoethanolamine (POPE), and cholesterol (Chol), were purchased from Avanti Polar Lipids, Inc. (Alabaster, AL, USA). The bovine eye lens α-crystallin, cholesterol analog cholestane spin-label (CSL), HEPES, and sodium chloride (NaCl) were purchased from Sigma Aldrich (St. Louis, MO, USA). The α-crystallin (C4163) was used without further purification. HEPES buffer (10 mM HEPES, 100 mM NaCl, pH = 7.4) was used to dissolve α-crystallin, prepare membranes, and prepare mixed α-crystallin and membrane samples for EPR measurements. The Sigma Aldrich provided information that αA = 19.8 kDa, αB = 22 kDa, and αA:αB = 3:1. Based on this information, the average molecular weight of the α-crystallin subunit was estimated to be 20.35 kDa.

2.2. Preparation of Small Unilamellar Vesicles (SUVs)

The PL, Chol, and CSL spin-label in chloroform solutions were mixed by maintaining 1 mol% CSL with respect to the lipids (PL plus Chol). The samples were prepared with varied Chol/PL mixing ratios 0, 0.1, 0.3, 0.5, 1.0, and 1.5. The mixed chloroform solutions were dried using a slow stream of N_2-gas to a final volume of ~75 μL. Then, ~400 μL of HEPES buffer (10 mM HEPES, 100 mM NaCl, pH = 7.4) was added to the solutions, and large multilamellar vesicles (LMVs) were prepared using the rapid solvent exchange method (RSEM) (Buboltz, 2009; Buboltz and Feigenson, 1999; Huang et al., 1999). The apparatus for the RSEM was built in our lab, as described in (Buboltz, 2009). The RSEM maintains the compositional homogeneity throughout the membrane suspensions (Buboltz and Feigenson, 1999; Huang et al., 1999). The small unilamellar vesicles (SUVs) were then prepared by sonication of LUVs using a probe-tip sonicator (Fisher Scientific, Model 550). Ten to fifteen 10 s sonication cycles followed by 15 s cooling in ice were sufficient to transform the milky LMV suspensions into the slight hazy transparent solutions of SUVs. The concentration of lipids (PL plus Chol) in the SUVs samples prepared by sonication was maintained at 33 mM. The protocol from Avanti Polar Lipids (Burgess, 1998) reported that the probe-tip sonication prepares SUVs with a diameter in the range of 15-50 nm. Based on this, we approximated the diameter of our SUVs ~30 nm (Mainali et al., 2015b; Timsina et al., 2021).

The SUVs were prepared from individual PLs (POPC, SM*, POPS, and POPE*, where * represents the presence of 20 mol% POPS) at Chol/PL mixing ratios 0, 0.1, 0.3, 0.5, 1.0, and 1.5. Due to the POPE molecules' negative curvature (Hamai et al., 2006), they form inverted micelles where the tails spread out and the headgroups bury inside the micelles (Tate et al., 1991). Therefore, we added 20 mol% POPS to 80 mol% POPE to prepare the POPE* membrane. We maintained this molar ratio for POPE* while preparing the Chol/POPE* membranes with mixing ratios 0, 0.1, and 0.5. Possibly due to Chol's strongest affinity to SM (McMullen et al., 2004), we could not obtain a slightly hazy transparent solution of SUVs by sonication of milky solutions of Chol/SM's LMVs, even at Chol/SM mixing ratio of 0.1. Therefore, we added 20 mol% of POPS to 80 mol% of SM to prepare the SM* membrane, and this molar ratio was maintained while preparing Chol/SM* membranes with mixing ratios 0, 0.3, 0.5, 1.0, and 1.5. The POPS is a charged phospholipid, for which preparation of SUVs by sonication is more favorable (Burgess et al., 1996). The addition of 20 mol% of POPS to the POPE and SM also makes the SUVs preparation by sonication more favorable, resulting in slightly hazy transparent solutions of SUVs.

Fig. 1 shows the schematic drawing of the distribution of CSL spin-labels in coexisting PCD and CBDs. The CSL spin-labels are particularly significant because they can locate and behave similarly to Chol molecules. The nitroxide moieties of CSL spin-labels are represented by black dots and are located near the membrane surface (see Fig. 1). The distinguishing feature of the CSL spin-labels is that they can uniformly distribute within coexisting PCD and CBDs, making it possible to probe the role of Chol in α-crystallin binding with the membrane. The blue highlighted region in Fig. 1 represents the CBD. CBDs are formed only after the membrane is saturated with Chol. CBDs start to form at 50, 48, 46, and 33 mol% Chol in the PC, SM, PS, and PE membranes, respectively (Mainali et al., 2020).

2.3. Binding of α-Crystallin to Small Unilamellar Vesicles (SUVs)

Each membrane sample was mixed with a varied concentration of α-crystallin by maintaining concentrations of lipids (PL plus Chol) 9.4 mM and α-crystallin from 0 to 52.6 μM. The total volume of the sample was 70 μL. The samples were then incubated at 37 °C for 16 h with gentle shaking in a Corning LSE benchtop shaking incubator (Corning, NY, USA). The binding of α-crystallin to the membranes is time-dependent, as evidenced by the time dependent-binding of α-crystallin to the POPC membranes, which saturates at ~8 h (Mainali et al., 2021). As we mentioned earlier, α-crystallin and membrane samples are stable at 37 °C for 16 h (Mainali et al., 2021; Timsina et al., 2021).

The native α-crystallin obtained from Sigma Aldrich might include a small proportion of other lens proteins. It has been reported that α-crystallin isolated from the bovine eye lens consists of ~6% other lens proteins (Horwitz et al., 1998; Ryazantsev et al., 2018). Therefore, in our case, there might be binding of other lens proteins with the membranes. As ~94% of the protein is α-crystallin, we suggest that the change in organization and dynamics of the

membrane sensed by CSL spin-labels incorporated into the membrane is likely due to the α-crystallin binding. Previously, no significant difference between the binding of native and the recombinant bovine α-crystallin with the synthetic PC 16:0 vesicles has been reported (Cobb and Petrash, 2002a).

2.4. EPR Measurements

The samples incubated at 37 °C for 16 h were filled into a 0.6 mm i.d. gas-permeable methylpentene polymer (TPX) capillary (Subczynski et al., 2005) for continuous-wave (CW) EPR measurements. An X-band Bruker ELEXSYS 500 spectrometer, connected with the accessories to control the temperature, was used to record the EPR spectra at 37 °C. Samples were thoroughly deoxygenated before taking EPR measurements. The modulation amplitude of 1.0 G and an incident microwave power of 5.0 mW was used to record the EPR spectra. For a single series of a sample, the EPR spectra were collected in a single day.

2.5. Measurements of Percentage of Membrane Surface Occupied (MSO) and Binding Affinity (K_a)

Each EPR spectrum was normalized with respect to peak to peak intensity of the spectrum's central line. The representative EPR spectra of SM* membrane with Chol/SM* mixing ratio of 0 and 1.5 are shown in Fig. 2A and C, respectively. The EPR spectra in black and red colors are without α-crystallin and with 52.6 μM α-crystallin, respectively. Fig. 2B and D represent the zoomed low field EPR lines of the spectra in Fig. 2A and C, respectively. The red-colored line in Fig. 2B shows that the low field EPR line's peak to peak intensity decreases due to the binding of α-crystallin to the SM* membrane. Previously, we observed a similar decrease in the low field line's peak to peak intensity due to the binding of α-crystallin to the individual POPC, SM, and POPS membranes as well as to two-component PLs mixtures SM/POPC, SM/POPS, and SM/POPE membranes (Mainali et al., 2021; Timsina et al., 2021). The red-colored line in Fig. 2D shows that the low field EPR line's peak to peak intensity remains the same as the black-colored line, indicating no binding of α-crystallin to the Chol/SM* membrane at the Chol/SM* mixing ratio of 1.5. Here, we use the change in the peak to peak intensity of the low field EPR line to calculate the K_a of α-crystallin to the Chol/PL membranes with varied Chol/PL mixing ratios from 0 to 1.5.

The detailed method to calculate the K_a of α-crystallin binding to the membranes, made of individual and two-component PL mixtures, using the EPR spin-labeling approach, is explained in our recent studies (Mainali et al., 2021; Timsina et al., 2021). Here, we use this recently developed method to estimate the K_a of α-crystallin binding to the Chol/POPC, Chol/SM*, Chol/POPS, and Chol/POPE* membranes with varied Chol/PL mixing ratios from 0 to 1.5. For each membrane with a fixed Chol/PL mixing ratio, peak to peak intensity of the low field EPR line without α-crystallin was used as a control representing the unbound contribution (U_0), and peak to peak intensity of the low field EPR line with α-crystallin was used as a bound plus unbound contribution ($B_0 + U_0$) (see Fig. 2B). Since the CSL spin-labels are near the surface of the membrane (close to the headgroup regions) and α-crystallin binds on the outer membrane surface, the percentage of CSL spin-labels affected due to the binding of α-crystallin was calculated as (Mainali et al., 2021; Timsina et al., 2021):

$$\%\ \text{CSL spin labels affected} = \{(U_0 - (B_0 + U_0)\}\,(U_0)^{-1}100\ \% \qquad (1)$$

As the membrane samples are SUVs with an approximate diameter of ~30 nm (Mainali et al., 2021, 2015b; Timsina et al., 2021), ~60% of the CSL molecules are near the outer membrane surface, and ~40% of the CSL molecules are near the inner membrane surface. Only the CSL molecules on the outer surface of the membrane are affected by the α-crystallin binding. Therefore, the corrected % CSL spin-labels affected due to α-crystallin binding or the MSO by α-crystallin is calculated by multiplying equation (1) by the correction factor (100/60):

$$\%\ \text{membrane surface occupied (MSO)} = (\%\ \text{CSL spin labels affected})\ (100/60) \qquad (2)$$

The MSO gives quantitative information about the percentage of the outer membrane surface occupied by the α-crystallin. The calculated MSO by α-crystallin were plotted as a function of α-crystallin concentration, and the data points were fitted using GraphPad Prism (San Diego, CA) with a one-site ligand binding model:

$$Y = (X\,B_{max})\,(K_d + X)^{-1} \quad (3)$$

Where B_{max} (maximum specific binding) is the extrapolation of the MSO by a very high concentration of α-crystallin, and K_d (dissociation constant) is the α-crystallin concentration needed to achieve a half-maximum binding at equilibrium. B_{max} has the same unit as Y, and K_d has the same unit as X. The α-crystallin can bind to any region of the membrane's outer surface with equal probability because the membranes' outer surface regions are identical. Thus, we used a one-site ligand binding model to estimate the K_d. The one-site ligand binding model was also used previously to estimate the K_a (Mainali et al., 2021; Schultz et al., 2017, 2013; Timsina et al., 2021). The association constant or the K_a is calculated as:

$$K_a = {K_d}^{-1} \quad (4)$$

Where the K_a gives information about how quickly the α-crystallin occupies the maximum surface of the membrane. For the same value of the MMSO by the α-crystallin, the value of K_a may differ depending on how quickly the MMSO is achieved. The K_a gives quantitative information about how quickly the MMSO is obtained. In other words, the K_a gives information about the strength of α-crystallin binding to membranes. The greater the value of K_a, the stronger is the α-crystallin binding to membranes and vice-versa.

The probe-tip sonication prepares SUVs with a diameter in the range of 15-50 nm (Burgess, 1998). Based on this, we approximated the diameter of our SUVs to be ~30 nm. Suppose our SUVs' diameter was not ~30 nm. In that case, the percentage of CSL spin-labels on the membranes' outer surface differs because of the change in the percentage of surface area covered by the membrane's outer surface with respect to the overall surface (inner plus outer). Due to this, we need to change the correction factor used to multiply equation (1) to obtain equation (2). This will make the value of the MSO by α-crystallin the same, as described previously (Timsina et al., 2021). For example, if the SUVs' diameter was ~200 nm, then ~52% of the CSL spin-labels reside near the outer membrane surface, which is smaller than ~60% CSL spin-labels in the case of SUVs with ~30 nm diameter. The decrease in the percentage of CSL spin-labels will be compensated by multiplying equation (1) by a larger correction factor of 100/52, which will make the MSO the same as in the ~30 nm diameter case. Therefore, we suggest that the MSO remains the same, even if the SUVs used are larger or smaller, as described previously (Timsina et al., 2021).

2.6. Measurements of Physical Properties of Membranes

The mobility parameter and maximum splitting of the membranes after α-crystallin binding were measured. The mobility parameter gives the orientational and rotational dynamics of the CSL spin-labels in the membranes (Schreier et al., 1978). The maximum splitting is related to the order parameter of the membrane, which gives the amplitude of the wobbling motion of the long axes of the CSL spin-labels in the membranes (Kusumi et al., 1986b; Mainali et al., 2012b; Raguz et al., 2011a). Due to the presence of CSL spin-labels on both the surfaces (inner and outer) of the membrane, the mobility parameter and maximum splitting give the average effect of CSL spin-labels contributing from both surfaces of the membrane. As explained before (Mainali et al., 2021, 2012b; Raguz et al., 2011a; Timsina et al., 2021), the ratio of peak to peak intensity of low field and central field EPR line (i.e., h_+/h_0) gives the mobility parameter (Fig. 2A), and the horizontal distance between the low and high field lines in the EPR spectra gives the maximum splitting (Fig. 2C).

2.7. Statistics

The Student's t-test was used to determine the statistical significance between the MMSO values and between the K_a values. The MMSO represents the values obtained after binding saturation. For the K_a, we used the values obtained from three independent experiments. The statistical significance was determined by comparing values (MMSO as well as K_a) among each other for the same membrane with different Chol/PL mixing ratios. A value of $p \leq 0.05$ was considered statistically significant.

3. Results and Discussion

3.1. MMSO by α-Crystallin on Chol/PL Membranes

The Chol/PL membrane, i.e., Chol/POPC or Chol/SM* or Chol/POPS or Chol/POPE*, with a lipids (PL plus Chol) concentration of 9.4 mM was mixed with a varied concentration of α-crystallin from 0 to 52.6 μM and incubated for 16 h at 37 °C with gentle shaking. The EPR measurements of incubated samples were performed at 37 °C. After taking EPR measurements, each spectrum was normalized with respect to peak to peak intensity of the central EPR line. Fig. 2A and C show the representative EPR spectra for the Chol/SM* membranes at Chol/SM* mixing ratios 0 and 1.5, respectively. In Fig. 2A and C, the black and the red colored spectra are in the absence of α-crystallin and presence of 52.6 μM α-crystallin, respectively. Fig. 2B and D show the zoomed low field EPR lines of the spectra in Fig. 2A and C, respectively. As shown in Fig. 2B, the peak to peak intensity of the low field EPR line of SM* membrane at Chol/SM* mixing ratio of 0 decreased in the presence of α-crystallin. Such a decrease in peak to peak intensity was due to the binding of α-crystallin to the SM* membrane. As shown in Fig. 3D, the peak to peak intensity of the low field EPR line of the Chol/SM* membrane at Chol/SM* mixing ratio 1.5 did not change in the presence of α-crystallin. It was due to no binding of α-crystallin to the Chol/SM* membrane at a Chol/SM* mixing ratio of 1.5.

The MSO was estimated by using equation (2). Fig. 3A, B, C, and D show the MSO by α-crystallin plotted as a function of α-crystallin concentration for the Chol/POPC, Chol/SM*, Chol/POPS, and Chol/POPE* membranes, respectively. The Chol/POPC, Chol/SM*, and Chol/POPS mixing ratios used were 0, 0.3, 0.5, 1.0, and 1.5, and the Chol/POPE* mixing ratios used were 0, 0.1, and 0.5. The data for the POPC membrane at Chol/POPC mixing ratio 0 (no Chol) and the POPS membrane at Chol/POPS mixing ratio 0 were taken from our recent studies (Mainali et al., 2021) and (Timsina et al., 2021), respectively. The binding of α-crystallin to the POPC and the SM* membranes was of special interest because PC is dominant in the lower-aged animals' lens, and SM is dominant in the human lens (Deeley et al., 2008). For the Chol/POPC, Chol/SM*, and Chol/POPS membranes, the MSO increased initially with an increase in the α-crystallin concentration, representing an increase in the binding of the α-crystallin to the membranes. At above certain α-crystallin concentration, the MSO remained the same, representing the saturation of α-crystallin binding to these membranes (Fig. 3A, B, and C). To the best of our knowledge, we are the first to measure the MSO by the α-crystallin. Without Chol in the membranes (Chol/PL mixing ratio of 0), the MMSO for the POPC, SM*, and POPS membranes were ~10, ~11.5, and ~11.2, respectively (see Fig. 3A, B, and C). It represents an almost equal amount of α-crystallin binds with the SM* and the POPS membranes; however, the lower amount of α-crystallin binds with the POPC membrane than with the SM* and the POPS membranes. Our results agreed with the previous observation that the higher amount of α-crystallin binds with the SM membrane than with the PC membrane (Tang et al., 1998). Previously, Mulders (Mulders et al., 1985) found ~10% α-crystallin bound to the egg yolk lecithin vesicles (PC vesicles) when α-crystallin labeled with [35S] methionine was incubated with the vesicles. Most importantly, the MMSO decreased with an increase in the Chol concentration for the Chol/POPC (Fig. 3A), Chol/SM* (Fig. 3B), and Chol/POPS (Fig. 3C) membranes, representing a lower amount of α-crystallin binding to the Chol/PL membranes with an increase in Chol content. For Chol/POPC membranes at the Chol/POPC mixing ratios 0, 0.3, 0.5, 1.0, and 1.5, the MMSO values were ~10, ~4.5, ~1.3, 0, and 0, respectively. For Chol/SM* membranes at the Chol/SM* mixing ratios 0, 0.3, 0.5, 1.0, and 1.5, the MMSO values were ~11.5, ~9, ~5.5, ~2, and 0, respectively. And, for the Chol/POPS membranes at the Chol/POPS mixing ratios 0, 0.3, 0.5, 1.0, and 1.5, the MMSO values were ~11.2, ~10.2, ~7.6, ~5, and ~3.4, respectively. Statistically significant differences were seen with $p \leq 0.05$ when the MMSO values of Chol/PL membranes at different Chol/PL mixing ratios were compared among each other. The data showed that the degree to which the MMSO decreases with an increase in Chol concentration was different for different PL membranes. The

decrease in the MMSO was quick for the Chol/POPC membrane (MMSO reached zero at the Chol/POPC mixing ratio of 1) than for the Chol/SM* membrane (MMSO reached zero at the Chol/SM* mixing ratio of 1.5). Interestingly, unlike for the Chol/POPC and the Chol/SM* membranes, the MMSO did not reach zero for the Chol/POPS membrane even at the Chol/POPS mixing ratio of 1.5. The MSO by α-crystallin on the Chol/POPE* membrane at all Chol/POPE* mixing ratios (0, 0.1, and 0.5) was zero, representing no α-crystallin binding to these membranes. Previously, we found zero MSO representing no binding of α-crystallin to the POPE* membrane (Timsina et al., 2021), where * represents the presence of 30 mol% POPC instead of 20 mol% POPS used in this study.

The outer surface of a membrane is identical, and α-crystallin can bind to any region of the membrane's outer surface with equal probability. If the binding of α-crystallin was limited to specific regions of the membrane's outer surface, the binding would have been saturated at a low concentration of α-crystallin. Our results (Fig. 3) showed the saturable binding of α-crystallin to the Chol/PL membranes at a high concentration of α-crystallin. Therefore, we think that the binding of α-crystallin to the Chol/PL membranes was non-specific. The α-crystallin remains in highly polydisperse oligomeric forms (Horwitz et al., 1998), and subunits exchange occurs between oligomers (Bova et al., 2000; Ryazantsev et al., 2018; Van den Oetelaar et al., 1990). Also, α-crystallin has hydrophobic regions on its surface (Mulders et al., 1985; Reddy et al., 2006). Our results suggest that the binding of α-crystallin to the Chol/PL membranes is hydrophobic in nature that occurs between the hydrophobic surface of the α-crystallin and the hydrophobic fatty acids core of the membranes. We think that only the hydrophobic regions (not the whole α-crystallin) exposed on the α-crystallin oligomers' surface contribute to the binding with the membranes. In this way, the CSL spin-labels on the membranes' outer surface may only be affected by the hydrophobic regions exposed on the surface of α-crystallin's oligomers. We think it is why the MMSO for all the Chol/PL membranes is small (Fig. 3). Additionally, the steric hindrance between the bound oligomers may also contribute to the smaller MMSO. The possibility of smaller oligomers binding with the Chol/PL membranes cannot be disregarded; however, the smaller oligomers might be less in numbers. Previously, our data of the interaction of α-crystallin with the Chol-free membranes made of individual and two-component PL mixtures of the eye lens PLs suggest hydrophobic interaction between α-crystallin and membranes (Timsina et al., 2021). Also, Cobb and Petrash (Cobb and Petrash, 2000) suggested a hydrophobic interaction between α-crystallin and the lens membrane. We have previously used CSL spin-labels and showed that with an increase in Chol content, there was a decrease in hydrophobicity (increase in polarity) near the surface of POPC and SM membranes (Mainali et al., 2011; Raguz et al., 2011a). Based on these observations and our data (Fig. 3), we suggest that with an increase in Chol content, the hydrophobicity near the membrane surface decreased (polarity increased), resulting in a decrease in hydrophobic interaction between α-crystallin and the hydrophobic fatty acid core of the membrane. That is why there was a significant reduction in the MMSO by α-crystallin with an increase in Chol content (see Fig. 3).

3.2. K_a for α-Crystallin Binding to Chol/PL Membranes

The K_a of α-crystallin binding to the Chol/PL membranes was estimated by fitting the MSO versus α-crystallin concentration data (shown in Fig. 3) using a one-site ligand binding model (equation 3). The solid lines connecting data points in Fig. 3 are fitted curves. Fig. 4A, B, and C show the K_a values for the Chol/POPC, Chol/SM*, and Chol/POPS membranes obtained from fitting the data shown in Fig. 3A, B, and C, respectively. The K_a for the POPC at Chol/POPC mixing ratio of 0 and the POPS at Chol/POPS mixing ratio of 0 were taken from our previous studies (Mainali et al., 2021) and (Timsina et al., 2021), respectively. The errors in the K_a values were estimated from three independent experiments. Statistically significant differences were observed with $p \leq 0.05$ when K_a values at different Chol/PL mixing ratios were compared among each other for the Chol/POPC, Chol/SM*, and Chol/POPS membranes. The zero MSO for the Chol/POPE* membranes at mixing ratios 0, 0.1, and 0.5 (Fig. 3D) represents no binding of α-crystallin to the Chol/POPE* membranes. Therefore, we did not show bar charts of the K_a (zero values) for the Chol/POPE* membranes. Previously, we observed no α-crystallin binding to the POPE* (* represents 30 mol% POPC, unlike 20 mol% POPS in this study) membrane (Timsina et al., 2021). Interestingly, with an increase in Chol/PL mixing ratio, a decrease in the K_a values was observed for the Chol/POPC, Chol/SM*, and Chol/POPS membranes. It represents that the strength of α-crystallin binding to the membranes decreased with an increase in Chol concentration in these membranes. Like MMSO (see Fig. 3), a sharp decrease in K_a was observed for the Chol/POPC membrane than for the Chol/SM* and Chol/POPS membranes (see Fig. 4). The K_a reached zero for the Chol/POPC membrane

when the Chol/POPC mixing ratio was 1.0, whereas for the Chol/SM* membrane K_a reached zero when the Chol/SM* mixing ratio was 1.5. However, the K_a did not reach zero even when the Chol/POPS mixing ratio in the Chol/POPS membrane was 1.5. These data represent that when Chol/POPC mixing ratio was 1.0 and Chol/SM* mixing ratio was 1.5, there was no binding of α-crystallin to the Chol/POPC and Chol/SM* membranes. However, there was α-crystallin binding to the Chol/POPS membrane even when the Chol/POPS mixing ratio was 1.5. Previously, Mulders (Mulders et al., 1985) estimated the K_a of 7.69 μM^{-1} to bind α-crystallin labeled with [35S] methionine to the alkali-washed lens plasma membranes. Our K_a values are slightly different from those reported in the literature, likely because our membranes include Chol and PL only, not the intrinsic proteins as in the lens plasma membranes used in the study reported in the literature.

Fig. 5 shows the schematic drawings of the organization of the Chol/POPC, Chol/SM*, Chol/POPS, and Chol/POPE* membranes with an increase in Chol content along with the schematics of α-crystallin bound to these membranes at different Chol/PL mixing ratios. PCD is the region where the membrane is saturated with Chol. With further increase of Chol content, CBDs are formed that coexist with surrounding PCD. The CBDs' formation within the membranes (Fig. 5) was estimated based on our previous study (Mainali et al., 2020), where we reported that CBDs start to form at 50, 48, 46, and 33 mol% Chol in the PC, SM, PS, and PE membranes, respectively. The schematics of α-crystallin bound to the membranes presented in Fig. 5 are drawn based on Fig. 3. Without Chol in the membranes (Chol/PL mixing ratio of 0), our data (Fig. 3) suggested that an almost similar amount of α-crystallin binds with the SM* and POPS membranes (as they have almost the same MMSO). However, the amount of α-crystallin binding with the POPC membranes was slightly lower than with the SM* and POPS membranes (Fig. 3) (as POPC have slightly lower MMSO than SM* and POPS). That is why a larger number of α-crystallin bound to the SM* and POPS membranes at 0 mol% Chol was shown than to the POPC membrane at 0 mol% Chol in Fig. 5. No binding of α-crystallin to the Chol/POPE* membranes was observed (Fig. 3D and Fig 5). With an increase in Chol concentration in the membranes, the binding of α-crystallin quickly decreased for the Chol/POPC membranes and slowly decreased for the Chol/POPS membranes (Fig. 5). Complete inhibition of α-crystallin binding was observed before the formation of CBDs within the Chol/POPC membranes and after the formation of CBDs within the Chol/SM* membranes. However, the binding of α-crystallin to the Chol/POPS membranes was not completely inhibited even after CBDs' formation at the Chol/POPS mixing ratio of 1.5 (see Fig. 5). Overall, our data showed that Chol and CBDs inhibit the binding of α-crystallin to the PL membranes. However, the degree of inhibition was different for the different PL membranes. These results suggest that the Chol and CBDs play a positive physiological role in preventing α-crystallin binding to the lens membranes.

The K_a of α-crystallin binding to PL membranes at the Chol/PL mixing ratio of 0 (no Chol) followed the trends: K_a (POPC) > K_a (SM*) > K_a (POPS) > K_a (POPE*) (Fig. 4). The data for the POPC membrane at Chol/POPC mixing ratio of 0 and the POPS membrane at Chol/POPS mixing ratio of 0 were taken from our previous studies (Mainali et al., 2021) and (Timsina et al., 2021), respectively. The K_a of α-crystallin binding to SM* membrane was about ten times smaller than to POPC membrane. However, the K_a of α-crystallin binding to SM* membrane was two times larger than to POPS membrane. Also, there was no binding of α-crystallin to the POPE* membranes, i.e., the K_a was zero. As suggested in our previous study (Timsina et al., 2021), we think that such a difference in K_a values is due to the difference in the capacity of PLs to modulate the hydrophobic interaction between α-crystallin and the hydrophobic fatty acid core of membranes, where PL headgroup's size and charge, hydrogen bonding between headgroups, and PL curvature plays a significant role.

With an increase in the Chol concentration, the MMSO and K_a decreased for the Chol/POPC, Chol/SM*, and Chol/POPS membranes (Fig. 3 and 4). Based on these data, we hypothesize that the increase in Chol content decreased the hydrophobicity (increased the polarity) near the surface of the Chol/PL membranes, which reduced the hydrophobic binding of α-crystallin to the hydrophobic fatty acid cores of the Chol/PL membranes. Previously, we used CSL spin-labels and observed a decrease in hydrophobicity near the surface of the SM (Mainali et al., 2011) and POPC (Raguz et al., 2011a) membranes with an increase in the Chol content in these membranes. Moreover, our data showed that the degree to which the MMSO and K_a decreased was different for different PL membranes (Fig. 3, 4, and 5). The decrease was quick for the Chol/POPC membrane and slow for the Chol/POPS membrane. It was likely due to the difference in the strength Chol interacts with different PLs. It was reported that the strength of Chol's interaction with PLs follows the trends: SM > PC > PS > PE (Ohvo-Rekilä et al., 2002). The SM has both an H-bond

acceptor and donor groups, and POPC has only an H-bond acceptor group. Both SM and POPC could form H-bonds with the Chol's -OH group (Boggs, 1987). In the Chol/POPC membrane, Chol molecules may directly H-bond to oxygen atoms in the POPC (M et al., 2000). There might also be water bridges between Chol's -OH groups and the oxygens in the POPC and might also have charge pairs between the Chol's -OH and POPC's choline moiety's -CH_3 groups (M et al., 2000). Due to these reasons, the binding of Chol and POPC molecules is strong. With an increase in Chol content in the Chol/POPC membrane, the strong binding of Chol and POPC likely decreases the hydrophobicity (increases polarity) near the surface of the Chol/POPC membrane quickly, reducing the hydrophobic interaction between α-crystallin and hydrophobic core of the membrane quickly. Likely due to this reason, with an increase in Chol content, the MMSO and K_a decreased quickly for the Chol/POPC membrane (Fig. 3A and 4A). For the Chol/POPS membrane, the presence of a negative charge in POPS's headgroup causes the POPS headgroups to repel one another, exposing the hydrophobic core. Simultaneously, the presence of Chol decreases the hydrophobicity (increase the polarity) near the surface of the Chol/POPS membrane (Raguz et al., 2011b). Likely due to these combined effects, the MMSO and K_a decrease slowly with an increase in Chol content in the Chol/POPS membrane, and the MMSO and K_a were not zero even at Chol/POPS mixing ratio of 1.5 (see Fig. 3C and 4C). For the Chol/SM* membrane, there might be a strong H-bond between SM's amide group and Chol's -OH group (Bittman et al., 1994). Also, with an increase in Chol content in Chol/SM membrane, the hydrophobicity near the membrane surface decreases slowly (Mainali et al., 2011) in comparison to Chol/POPC membrane, for which the decrease in hydrophobicity near the membrane surface is sharp (Raguz et al., 2011a). Likely due to these reasons, the MMSO and K_a for the Chol/SM* membrane decrease slower than for the Chol/POPC membrane, for which MMSO and K_a become zero at lower Chol content (i.e., Chol/POPC mixing ratio of 1.0). However, the MMSO and K_a become zero comparatively at higher Chol content for the Chol/SM* membrane (i.e., Chol/SM* mixing ratio of 1.5). An important point to note is that irrespective of the PL type, our data suggest that the MMSO and K_a decrease with an increase in Chol concentration, implying that Chol and CBDs inhibit α-crystallin binding to membranes that likely help to maintain the lens transparency. Based on our data, an increase in lens transparency with an increase in Chol content is shown by the arrow in the schematic in Fig. 5.

3.3. Mobility Parameter of Chol/PL Membranes After α-Crystallin Binding

The mobility parameter of the Chol/PL (Chol/POPC, Chol/SM*, Chol/POPS, and Chol/POPE*) membranes after α-crystallin binding were calculated using the method explained in section 2.6. Fig. 6A, B, and C show the profiles of mobility parameters plotted as a function of α-crystallin concentration for the Chol/POPC, Chol/SM*, and Chol/POPS membranes, respectively, at mixing ratios 0, 0.3, 0.5, 1.0, and 1.5. Fig. 6D shows the profiles of mobility parameters plotted as a function of α-crystallin concentration for the Chol/POPE* membrane at mixing ratios 0, 0.1, and 0.5. The data for the POPC membrane at Chol/POPC mixing ratio of 0 and the POPS membrane at Chol/POPS mixing ratio of 0 were taken from our previous studies (Mainali et al., 2021) and (Timsina et al., 2021), respectively. The error bars were estimated from the three independent experiments. Without Chol (Chol/PL mixing ratio of 0) and α-crystallin (0 μM α-crystallin), the mobility parameter of the membranes followed the trends: POPC > POPS > SM* > POPE*. It represents that the orientational and rotational dynamics of the CSL spin-labels were largest in the POPC membrane and smallest in the POPE* membrane. Since the CSL spin-labels reside near the lipids' headgroup regions in the membranes (see Fig. 1), the mobility parameter can be understood as mobility near the membranes' headgroup regions. Therefore, our results implied that the mobility near the headgroup regions was largest in the POPC membrane and smallest in the POPE* membrane. With an increase in the α-crystallin concentration, the mobility parameter decreased for the POPC, SM*, and POPS (Fig 6A, B, and C) membranes. It represents that the membranes near the headgroup regions became more immobilized due to the binding of α-crystallin to these membranes. There was no change in the POPE* membrane's mobility parameter because of no binding of α-crystallin to the POPE* membrane. With the inclusion of Chol in the membranes, two significant effects have been observed. First, the membranes' mobility parameter decreased with an increase in the Chol concentration in the membranes. For example, the Chol/POPC membranes with mixing ratios of 0 and 1.5 have the highest and the lowest mobility parameter, respectively (Fig. 6A). A similar effect was observed for the Chol/SM*, Chol/POPS, and Chol/POPE* membranes, as shown in Fig. 6B, C, and D, respectively. Second, the decrease in mobility parameter with an increase in the α-crystallin concentration was less pronounced with an increase in Chol concentration in the Chol/POPC, Chol/SM*, and Chol/POPS membranes. When the Chol/POPC mixing ratio reached 1.0 in the Chol/POPC membrane and the Chol/SM* mixing ratio reached

1.5 in the Chol/SM* membrane, there was no change in the mobility parameter with an increase in the α-crystallin concentration. However, a small decrease in the mobility parameter with the increase in α-crystallin concentration was observed for the Chol/POPS membrane even at the Chol/POPS mixing ratio of 1.5. No change in the mobility parameter was observed in the Chol/POPE* membrane because there was no binding of α-crystallin to this membrane. In combination, the observed two effects imply that an increase in Chol concentration in the membranes decreases the membranes' mobility near the headgroup regions and antagonizes the capacity of the α-crystallin to decrease mobility near the headgroup regions. Because less amount of α-crystallin binds with the membrane with an increase in Chol concentration, the ability of α-crystallin to decrease the mobility near the headgroup regions becomes less with increasing Chol content in the membranes. Previously, Borchman and Tang (1996) used fluorophore NBD-PE, which partitions near the membrane's headgroup regions, and found a decrease in the headgroup mobility of the bovine lens lipid vesicles upon α-crystallin binding.

Our data suggest that the sharpness of the mobility parameter decrease depends on the K_a (or strength) of α-crystallin binding with the membranes. The higher the K_a, the sharp is the mobility parameter decrease, and vice-versa. For example, the mobility parameter decreases sharply for POPC membrane at Chol/POPC mixing ratio of 0 and slowly for the POPS membrane at Chol/POPS mixing ratio of 0 because the K_a of α-crystallin binding to the Chol/POPC membrane is the largest and to Chol/POPS is the least. The data for all Chol/PL membranes at different Chol/PL mixing ratios support this claim. Moreover, our data suggest that the overall decrease of the mobility parameter depends on the MMSO by the α-crystallin. The higher the MMSO, the higher is the overall decrease of the mobility parameter and vice-versa. For example, the overall decrease in the mobility parameter is highest for the SM* membrane at the Chol/SM* mixing ratio of 0 because the MMSO by α-crystallin is the highest (~11.5%) for this membrane.

3.4. Maximum Splitting of Chol/PL Membranes After α-Crystallin Binding

The maximum splitting of the Chol/PL (Chol/POPC, Chol/SM*, Chol/POPS, and Chol/POPE*) membranes after α-crystallin binding were calculated using the method explained in section 2.6. Fig. 7A, B, and C show the maximum splitting plotted as a function of α-crystallin concentration for the Chol/POPC, Chol/SM*, and Chol/POPS membranes, respectively, at Chol/PL mixing ratios 0, 0.3, 0.5, 1.0, and 1.5. Fig. 7D shows the maximum splitting plotted as a function of α-crystallin concentration for the Chol/POPE* membranes at Chol/POPE* mixing ratio of 0, 0.1, and 0.5. The data for the POPC membrane at the Chol/POPC mixing ratio of 0 and the POPS membrane at the Chol/POPS mixing ratio of 0 were taken from our previous studies (Mainali et al., 2021) and (Timsina et al., 2021), respectively. Without Chol (Chol/PL mixing ratio of 0) and α-crystallin (at 0 μM α-crystallin), the maximum splitting of the membranes followed the trends: SM* > POPE* > POPS > POPC. It represents that the SM* membrane has the highest order near the headgroup regions and the POPC membrane has the lowest order near the headgroup regions. A decrease in the amount of PC and an increase in the amount of SM is expected in the lens membranes during aging (Borchman et al., 1994; Yappert et al., 2003). Our observation representing the highest order near the headgroup regions of the SM* membrane and lowest order near the headgroup regions of the POPC membranes support the increased order of the lens lipids (Borchman et al., 2004, 1999) with aging. Without Chol in the membranes, the trends of the maximum splitting were the same as the trends of the MMSO (i.e., SM* > POPS > POPC). It helps to speculate that an ordered membrane can bind a higher amount of α-crystallin. Interestingly, with an increase in the Chol concentration in the membranes, the maximum splitting increased. It represents that Chol increases the order near the headgroup regions of the membranes. The higher the Chol concentration in the membranes (i.e., the higher the Chol/PL mixing ratio), the higher is the maximum splitting or the order near the headgroup regions of the membrane and vice-versa. Surprisingly, we observed no significant change in the maximum splitting with an increase in α-crystallin concentration (see Fig. 7), representing no significant change of the membrane's order near the headgroup regions. Previously, we observed an increased order near the headgroup regions of the SM and SM/POPE (70:30 mol%) membranes with an increase in α-crystallin concentration (Timsina et al., 2021).

4. Conclusions

In conclusion, we performed EPR measurements to probe the Chol and CBDs' role on α-crystallin binding to Chol/POPC, Chol/SM*, Chol/POPS, and Chol/POPE* membranes (* represents the presence of 20 mol% POPS) prepared with varied Chol/PL mixing ratio from 0 to 1.5. The advantage of using lipids (PL and Chol) only is that there are no intrinsic proteins, such as MIP26, that may change the interaction of α-crystallin with the membranes. Therefore, it helps investigate the influence of individual PL and Chol on the interaction of α-crystallin with the membranes. We reported the K_a of α-crystallin binding to membranes, the MMSO by α-crystallin, and the change in mobility parameter and maximum splitting of the membranes after α-crystallin binding. The values of K_a and MMSO decreased with an increase in Chol concentration for the Chol/POPC, Chol/SM*, and Chol/POPS membranes; however, the decrease in these values is different for different PL membranes. For the Chol/POPC membrane, both the K_a and MMSO decrease with an increase in Chol concentration and eventually reach zero at Chol/POPC mixing ratio of 1.0 (50 mol% Chol), representing complete inhibition of the α-crystallin binding to Chol/POPC membrane before CBDs start to form in the membrane. For the Chol/SM* membrane, both the K_a and MMSO decrease with an increase in Chol concentration and eventually reach zero at Chol/SM* mixing ratio of 1.5, representing that Chol completely inhibits the α-crystallin binding to Chol/SM* membrane when CBDs formed in the membrane. For the Chol/POPS membrane, both the K_a and MMSO decrease with an increase in Chol concentration; however, the values did not reach zero even at the Chol/POPS mixing ratio of 1.5. It represents that Chol could not completely inhibit the α-crystallin binding to the Chol/POPS membrane even after the formation of CBDs at the Chol/POPS mixing ratio of 1.5. For the Chol/POPE* membrane, both the K_a and MMSO were zero for Chol/POPE* mixing ratios 0, 0.1, and 0.5, representing no α-crystallin binding to the Chol/POPE* membrane with and without Chol. The results demonstrate that Chol and CBDs inhibit the α-crystallin binding to PL membranes; however, the degree of inhibition depends on the type of PL in the membrane. The outer surface of the Chol/PL membrane is identical. Therefore, α-crystallin can bind to any region of the Chol/PL membrane's outer surface with equal probability. If α-crystallin binds to specific regions of the Chol/PL membrane's outer surface, the binding could have been saturated even at a low concentration of α-crystallin; however, the concentration of α-crystallin was high (see Fig. 3). Therefore, we speculate that α-crystallin binds to the Chol/PL membrane non-specifically. Since the MMSO by α-crystallin is small (see Fig. 3), we speculate that only hydrophobic regions of the α-crystallin that are exposed on the outer surface of the α-crystallin oligomer contribute to the hydrophobic binding of α-crystallin with the Chol/PL membrane. This suggests that if the surface area of hydrophobic regions of the α-crystallin exposed on the outer surface α-crystallin oligomer is large, the amount of α-crystallin binding to the Chol/PL membrane (or MMSO) may also be large.

The membranes' mobility parameter profiles decreased with an increase in α-crystallin concentration, but the decrease was more pronounced for a low concentration of Chol in the membranes. It implies that membranes near the headgroup regions become more immobilized, with an increase in α-crystallin binding. However, the ability of α-crystallin to immobilize membrane near the headgroup regions decreases with an increase in Chol concentration. The maximum splitting profiles of all the membranes did not change significantly with an increase in α-crystallin concentration; however, there was an increase in the maximum splitting values with an increase in Chol concentration in the membranes. It implies that the increase in Chol concentration in membranes increases the membranes' order near the headgroup regions, but there was no significant difference in the membrane order near the headgroup regions with an increase in α-crystallin concentration. Although we did not replicate the in-vivo conditions of the lens membranes and α-crystallin, the data obtained help to extrapolate that Chol and CBDs inhibit the binding of α-crystallin to the lens membranes and modulate the capacity of α-crystallin to change the physical properties of the membranes. In the adult human eye lens, the PL composition is 66% sphingolipids (SM plus DHSM), 11% PC, 8% PS, and 15% PE (Deeley et al., 2008). The Chol/PL molar ratio in the human eye lens membrane is as high as 1.8 in cortical membranes and 4.4 in the nuclear membranes (Boggs, 1987; Mainali et al., 2017; Truscott, 2000; Widomska and Subczynski, 2019). Therefore, our data suggest that Chol and CBDs formed at high Chol content likely inhibit the binding of α-crystallin to the human lens membranes. Thus, this study provides the molecular basics of understanding the high Chol's functions in the fiber cell plasma membrane of the eye lens, preventing the binding of α-crystallin to the lens membranes and possibly protecting against cataract formation and progression.

Author Declaration

The authors report no conflicts of interest.

Acknowledgements

Research reported in this publication was supported by the National Institutes of Health (USA) under Grant R01 EY030067.

References

Bassnett, S., Shi, Y., Vrensen, G.F.J.M., 2011. Biological glass: structural determinants of eye lens transparency. Philos. Trans. R. Soc. B Biol. Sci. 366, 1250–1264. https://doi.org/10.1098/rstb.2010.0302

Biswas, S.K., Jiang, J.X., Lo, W.-K., 2009. Gap junction remodeling associated with cholesterol redistribution during fiber cell maturation in the adult chicken lens. Mol. Vis. 15, 1492–1508.

Biswas, S.K., Lee, J.E., Brako, L., Jiang, J.X., Lo, W.-K., 2010. Gap junctions are selectively associated with interlocking ball-and-sockets but not protrusions in the lens. Mol. Vis. 16, 2328–2341.

Biswas, S.K., Lo, W.-K., 2007. Gap junctions contain different amounts of cholesterol which undergo unique sequestering processes during fiber cell differentiation in the embryonic chicken lens. Mol. Vis. 13, 345–359.

Bittman, R., Kasireddy, C.R., Mattjus, P., Slotte, J.P., 1994. Interaction of Cholesterol with Sphingomyelin in Monolayers and Vesicles. Biochemistry 33, 11776–11781. https://doi.org/10.1021/bi00205a013

Boggs, J.M., 1987. Lipid intermolecular hydrogen bonding: influence on structural organization and membrane function. Biochim. Biophys. Acta 906, 353–404. https://doi.org/10.1016/0304-4157(87)90017-7

Borchman, D., 2020. Lipid Conformational Order and the Etiology of Cataract and Dry Eye. J. Lipid Res. https://doi.org/10.1194/jlr.tr120000874

Borchman, D., Byrdwell, W.C., Yappert, M.C., 1994. Regional and age-dependent differences in the phospholipid composition of human lens membranes. Invest. Ophthalmol. Vis. Sci. 35, 3938–3942.

Borchman, D., Cenedella, R.J., Lamba, O.P., 1996. Role of cholesterol in the structural order of lens membrane lipids. Exp. Eye Res. 62, 191–197. https://doi.org/10.1006/exer.1996.0023

Borchman, D., Delamere, N.A., McCauley, L.A., Paterson, C.A., 1989. Studies on the distribution of cholesterol, phospholipid, and protein in the human and bovine lens. Lens Eye Toxic. Res. 6, 703–724.

Borchman, D., Stimmelmayr, R., George, J.C., 2017. Whales, lifespan, phospholipids, and cataracts. J. Lipid Res. 58, 2289–2298. https://doi.org/10.1194/jlr.M079368

Borchman, D., Tang, D., 1996. Binding capacity of alpha-crystallin to bovine lens lipids. Exp. Eye Res. 63, 407–410. https://doi.org/10.1006/exer.1996.0130

Borchman, D., Tang, D., Yappert, M.C., 1999. Lipid composition, membrane structure relationships in lens and muscle sarcoplasmic reticulum membranes. Biospectroscopy 5, 151–167. https://doi.org/10.1002/(SICI)1520-6343(1999)5:3<151::AID-BSPY5>3.0.CO;2-D

Borchman, D., Yappert, M.C., 2010. Lipids and the ocular lens. J. Lipid Res. 51, 2473–2488. https://doi.org/10.1194/jlr.R004119

Borchman, D., Yappert, M.C., Afzal, M., 2004. Lens lipids and maximum lifespan. Exp. Eye Res., Dr Abraham Spector International Symposium 79, 761–768. https://doi.org/10.1016/j.exer.2004.04.004

Bova, M.P., Mchaourab, H.S., Han, Y., Fung, B.K.-K., 2000. Subunit Exchange of Small Heat Shock Proteins ANALYSIS OF OLIGOMER FORMATION OF αA-CRYSTALLIN AND Hsp27 BY FLUORESCENCE RESONANCE ENERGY TRANSFER AND SITE-DIRECTED TRUNCATIONS. J. Biol. Chem. 275, 1035–1042. https://doi.org/10.1074/jbc.275.2.1035

Boyle, D.L., Takemoto, L., 1996. EM immunolocalization of α-crystallins: Association with the plasma membrane from normal and cataractous human lenses. Curr. Eye Res. 15, 577–582. https://doi.org/10.3109/02713689609000769

Brown, D.A., London, E., 2000. Structure and function of sphingolipid- and cholesterol-rich membrane rafts. J. Biol. Chem. 275, 17221–17224. https://doi.org/10.1074/jbc.R000005200

Buboltz, J.T., 2009. A more efficient device for preparing model-membrane liposomes by the rapid solvent exchange method. Rev. Sci. Instrum. 80, 124301. https://doi.org/10.1063/1.3264073

Buboltz, J.T., Feigenson, G.W., 1999. A novel strategy for the preparation of liposomes: rapid solvent exchange. Biochim. Biophys. Acta 1417, 232–245. https://doi.org/10.1016/s0005-2736(99)00006-1

Burgess, S., 1998. Liposome Preparation - Avanti® Polar Lipids [WWW Document]. Sigma-Aldrich. URL https://www.sigmaaldrich.com/technical-documents/articles/biology/liposome-preparation.html.

Burgess, S., Moore, J., Shaw, W., 1996. Avanti® FAQ [WWW Document]. Sigma-Aldrich. URL https://www.sigmaaldrich.com/technical-documents/articles/biology/avanti-faq.html.

Cenedella, R.J., Fleschner, C.R., 1992. Selective association of crystallins with lens “native” membrane during dynamic cataractogenesis. Curr. Eye Res. 11, 801–815. https://doi.org/10.3109/02713689209000753

Chandrasekher, G., Cenedella, R.J., 1997. Properties of alpha-crystallin bound to lens membrane: probing organization at the membrane surface. Exp. Eye Res. 64, 423–430. https://doi.org/10.1006/exer.1996.0228

Chandrasekher, G., Cenedella, R.J., 1995. Protein associated with human lens “native” membrane during aging and cataract formation. Exp. Eye Res. 60, 707–717. https://doi.org/10.1016/s0014-4835(05)80012-0

Cobb, B.A., Petrash, J.M., 2002a. Factors influencing α-crystallin association with phospholipid vesicles. Mol. Vis. 8, 85–93.

Cobb, B.A., Petrash, J.M., 2002b. alpha-Crystallin chaperone-like activity and membrane binding in age-related cataracts. Biochemistry 41, 483–490. https://doi.org/10.1021/bi0112457

Cobb, B.A., Petrash, J.M., 2000. Characterization of alpha-crystallin-plasma membrane binding. J. Biol. Chem. 275, 6664–6672. https://doi.org/10.1074/jbc.275.9.6664

Cooper, G.M., 2000. Structure of the Plasma Membrane. Cell Mol. Approach 2nd Ed.

Daly, T., Wang, M., Regen, S.L., 2011. The Origin of Cholesterol’s Condensing Effect. Langmuir ACS J. Surf. Colloids 27, 2159–2161. https://doi.org/10.1021/la105039q

Datiles, M.B., Ansari, R.R., Yoshida, J., Brown, H., Zambrano, A.I., Tian, J., Vitale, S., Zigler, J.S., Ferris, F.L., West, S.K., Stark, W.J., 2016. Longitudinal Study of Age Related Cataract Using Dynamic Light Scattering: Loss of α-crystallin Leads to Nuclear Cataract Development. Ophthalmology 123, 248–254. https://doi.org/10.1016/j.ophtha.2015.10.007

de Almeida, R.F.M., Fedorov, A., Prieto, M., 2003. Sphingomyelin/Phosphatidylcholine/Cholesterol Phase Diagram: Boundaries and Composition of Lipid Rafts. Biophys. J. 85, 2406–2416.

Deeley, J.M., Mitchell, T.W., Wei, X., Korth, J., Nealon, J.R., Blanksby, S.J., Truscott, R.J.W., 2008. Human lens lipids differ markedly from those of commonly used experimental animals. Biochim. Biophys. Acta 1781, 288–298. https://doi.org/10.1016/j.bbalip.2008.04.002

Emmelot, P., 1977. 1 - The organization of the plasma membrane of mammalian cells: structure in relation to function, in: Jamieson, G.A., Robinson, D.M. (Eds.), The Diversity of Membrane. Butterworth-Heinemann, pp. 1–54. https://doi.org/10.1016/B978-0-408-70723-7.50006-7

Friedrich, M.G., Truscott, R.J.W., 2010. Large-scale binding of α-crystallin to cell membranes of aged normal human lenses: a phenomenon that can be induced by mild thermal stress. Invest. Ophthalmol. Vis. Sci. 51, 5145–5152. https://doi.org/10.1167/iovs.10-5261

Fu, S.C., Su, S.W., Wagner, B.J., Hart, R., 1984. Characterization of lens proteins. IV. Analysis of soluble high molecular weight protein aggregates in human lenses. Exp. Eye Res. 38, 485–495. https://doi.org/10.1016/0014-4835(84)90126-x

Grami, V., Marrero, Y., Huang, L., Tang, D., Yappert, M.C., Borchman, D., 2005. alpha-Crystallin binding in vitro to lipids from clear human lenses. Exp. Eye Res. 81, 138–146. https://doi.org/10.1016/j.exer.2004.12.014

Hamai, C., Yang, T., Kataoka, S., Cremer, P.S., Musser, S.M., 2006. Effect of Average Phospholipid Curvature on Supported Bilayer Formation on Glass by Vesicle Fusion. Biophys. J. 90, 1241–1248. https://doi.org/10.1529/biophysj.105.069435

Horwitz, J., 2003. Alpha-crystallin. Exp. Eye Res. 76, 145–153. https://doi.org/10.1016/s0014-4835(02)00278-6

Horwitz, J., Bova, M.P., Ding, L.L., Haley, D.A., Stewart, P.L., 1999. Lens alpha-crystallin: function and structure. Eye Lond. Engl. 13 (Pt 3b), 403–408. https://doi.org/10.1038/eye.1999.114

Horwitz, J., Huang, Q.L., Ding, L., Bova, M.P., 1998. Lens alpha-crystallin: chaperone-like properties. Methods Enzymol. 290, 365–383. https://doi.org/10.1016/s0076-6879(98)90032-5

Huang, J., Buboltz, J.T., Feigenson, G.W., 1999. Maximum solubility of cholesterol in phosphatidylcholine and phosphatidylethanolamine bilayers. Biochim. Biophys. Acta 1417, 89–100. https://doi.org/10.1016/s0005-2736(98)00260-0

Huang, L., Grami, V., Marrero, Y., Tang, D., Yappert, M.C., Rasi, V., Borchman, D., 2005. Human Lens Phospholipid Changes with Age and Cataract. Invest. Ophthalmol. Vis. Sci. 46, 1682–1689. https://doi.org/10.1167/iovs.04-1155

Hung, W.-C., Lee, M.-T., Chen, F.-Y., Huang, H.W., 2007. The condensing effect of cholesterol in lipid bilayers. Biophys. J. 92, 3960–3967. https://doi.org/10.1529/biophysj.106.099234

Ifeanyi, F., Takemoto, L., 1991. Interaction of lens crystallins with lipid vesicles. Exp. Eye Res. 52, 535–538. https://doi.org/10.1016/0014-4835(91)90054-i

Ikeda, M., Longnecker, R., 2007. Cholesterol is critical for Epstein-Barr virus latent membrane protein 2A trafficking and protein stability. Virology 360, 461–468. https://doi.org/10.1016/j.virol.2006.10.046

Incardona, J.P., Eaton, S., 2000. Cholesterol in signal transduction. Curr. Opin. Cell Biol. 12, 193–203. https://doi.org/10.1016/s0955-0674(99)00076-9

Jacob, R.F., Cenedella, R.J., Mason, R.P., 2001. Evidence for distinct cholesterol domains in fiber cell membranes from cataractous human lenses. J. Biol. Chem. 276, 13573–13578. https://doi.org/10.1074/jbc.M010077200

Kusumi, A., Subczynski, W.K., Pasenkiewicz-Gierula, M., Hyde, J.S., Merkle, H., 1986a. Spin-label studies on phosphatidylcholine-cholesterol membranes: effects of alkyl chain length and unsaturation in the fluid phase. Biochim. Biophys. Acta 854, 307–317. https://doi.org/10.1016/0005-2736(86)90124-0

Kusumi, A., Subczynski, W.K., Pasenkiewicz-Gierula, M., Hyde, J.S., Merkle, H., 1986b. Spin-label studies on phosphatidylcholine-cholesterol membranes: effects of alkyl chain length and unsaturation in the fluid phase. Biochim. Biophys. Acta 854, 307–317. https://doi.org/10.1016/0005-2736(86)90124-0

Lampi, K.J., Ma, Z., Hanson, S.R., Azuma, M., Shih, M., Shearer, T.R., Smith, D.L., Smith, J.B., David, L.L., 1998. Age-related changes in human lens crystallins identified by two-dimensional electrophoresis and mass spectrometry. Exp. Eye Res. 67, 31–43. https://doi.org/10.1006/exer.1998.0481

Li, L.K., So, L., Spector, A., 1987. Age-dependent changes in the distribution and concentration of human lens cholesterol and phospholipids. Biochim. Biophys. Acta 917, 112–120. https://doi.org/10.1016/0005-2760(87)90291-8

M, P.-G., T, R., K, K., A, K., 2000. Cholesterol effects on the phosphatidylcholine bilayer polar region: a molecular simulation study. Biophys. J. 78, 1376–1389. https://doi.org/10.1016/s0006-3495(00)76691-4

Ma, Z., Hanson, S.R., Lampi, K.J., David, L.L., Smith, D.L., Smith, J.B., 1998. Age-related changes in human lens crystallins identified by HPLC and mass spectrometry. Exp. Eye Res. 67, 21–30. https://doi.org/10.1006/exer.1998.0482

Mainali, L., O'Brien, W.J., Subczynski, W.K., 2019. Detection of cholesterol bilayer domains in intact biological membranes: Methodology development and its application to studies of eye lens fiber cell plasma membranes. Exp. Eye Res. 178, 72–81. https://doi.org/10.1016/j.exer.2018.09.020

Mainali, L., O'Brien, W.J., Timsina, R., 2021. Interaction of Alpha-Crystallin with Phospholipid Membranes. Curr. Eye Res. 46, 185–194. https://doi.org/10.1080/02713683.2020.1786131

Mainali, L., Pasenkiewicz-Gierula, M., Subczynski, W.K., 2020. Formation of cholesterol Bilayer Domains Precedes Formation of Cholesterol Crystals in Membranes Made of the Major Phospholipids of Human Eye Lens Fiber Cell Plasma Membranes. Curr. Eye Res. 45, 162–172. https://doi.org/10.1080/02713683.2019.1662058

Mainali, L., Raguz, M., O'Brien, W.J., Subczynski, W.K., 2017. Changes in the Properties and Organization of Human Lens Lipid Membranes Occurring with Age. Curr. Eye Res. 42, 721–731. https://doi.org/10.1080/02713683.2016.1231325

Mainali, L., Raguz, M., O'Brien, W.J., Subczynski, W.K., 2015a. Properties of membranes derived from the total lipids extracted from clear and cataractous lenses of 61–70-year-old human donors. Eur. Biophys. J. EBJ 44, 91–102. https://doi.org/10.1007/s00249-014-1004-7

Mainali, L., Raguz, M., O'Brien, W.J., Subczynski, W.K., 2013. Properties of Membranes Derived from the Total Lipids Extracted from the Human Lens Cortex and Nucleus. Biochim. Biophys. Acta 1828, 1432–1440. https://doi.org/10.1016/j.bbamem.2013.02.006

Mainali, L., Raguz, M., O'Brien, W.J., Subczynski, W.K., 2012a. Properties of fiber cell plasma membranes isolated from the cortex and nucleus of the porcine eye lens. Exp. Eye Res. 97, 117–129. https://doi.org/10.1016/j.exer.2012.01.012

Mainali, L., Raguz, M., Subczynski, W.K., 2012b. Phases and domains in sphingomyelin-cholesterol membranes: structure and properties using EPR spin-labeling methods. Eur. Biophys. J. EBJ 41, 147–159. https://doi.org/10.1007/s00249-011-0766-4

Mainali, L., Raguz, M., Subczynski, W.K., 2011. Phase-Separation and Domain-Formation in Cholesterol-Sphingomyelin Mixture: Pulse-EPR Oxygen Probing. Biophys. J. 101, 837–846. https://doi.org/10.1016/j.bpj.2011.07.014

Mainali, L., Vasquez-Vivar, J., Hyde, J.S., Subczynski, W.K., 2015b. Spin-labeled small unilamellar vesicles with the T1-sensitive saturation-recovery EPR display as an oxygen sensitive analyte for measurement of cellular respiration. Appl. Magn. Reson. 46, 885–895. https://doi.org/10.1007/s00723-015-0684-1

McMullen, T.P.W., Lewis, R.N.A.H., McElhaney, R.N., 2004. Cholesterol–phospholipid interactions, the liquid-ordered phase and lipid rafts in model and biological membranes. Curr. Opin. Colloid Interface Sci. 8, 459–468. https://doi.org/10.1016/j.cocis.2004.01.007

Mulders, J.W., Stokkermans, J., Leunissen, J.A., Benedetti, E.L., Bloemendal, H., de Jong, W.W., 1985. Interaction of alpha-crystallin with lens plasma membranes. Affinity for MP26. Eur. J. Biochem. 152, 721–728. https://doi.org/10.1111/j.1432-1033.1985.tb09253.x

Ohvo-Rekilä, H., Ramstedt, B., Leppimäki, P., Peter Slotte, J., 2002. Cholesterol interactions with phospholipids in membranes. Prog. Lipid Res. 41, 66–97. https://doi.org/10.1016/S0163-7827(01)00020-0

Paterson, C.A., Zeng, J., Husseini, Z., Borchman, D., Delamere, N.A., Garland, D., Jimenez-Asensio, J., 1997. Calcium ATPase activity and membrane structure in clear and cataractous human lenses. Curr. Eye Res. 16, 333–338. https://doi.org/10.1076/ceyr.16.4.333.10689

Raguz, M., Mainali, L., Widomska, J., Subczynski, W.K., 2011a. Using spin-label electron paramagnetic resonance (EPR) to discriminate and characterize the cholesterol bilayer domain. Chem. Phys. Lipids 164, 819–829. https://doi.org/10.1016/j.chemphyslip.2011.08.001

Raguz, M., Mainali, L., Widomska, J., Subczynski, W.K., 2011b. The immiscible cholesterol bilayer domain exists as an integral part of phospholipid bilayer membranes. Biochim. Biophys. Acta BBA - Biomembr. 1808, 1072–1080. https://doi.org/10.1016/j.bbamem.2010.12.019

Raguz, M., Widomska, J., Dillon, J., Gaillard, E.R., Subczynski, W.K., 2009. Physical properties of the lipid bilayer membrane made of cortical and nuclear bovine lens lipids: EPR spin-labeling studies. Biochim. Biophys. Acta 1788, 2380–2388. https://doi.org/10.1016/j.bbamem.2009.09.005

Reddy, G.B., Kumar, P.A., Kumar, M.S., 2006. Chaperone-like activity and hydrophobicity of alpha-crystallin. IUBMB Life 58, 632–641. https://doi.org/10.1080/15216540601010096

Rituper, B., Flašker, A., Guček, A., Chowdhury, H.H., Zorec, R., 2012. Cholesterol and regulated exocytosis: A requirement for unitary exocytotic events. Cell Calcium, REGULATED EXOCYSTOSIS 52, 250–258. https://doi.org/10.1016/j.ceca.2012.05.009

Rujoi, M., Jin, J., Borchman, D., Tang, D., Yappert, M.C., 2003. Isolation and Lipid Characterization of Cholesterol-Enriched Fractions in Cortical and Nuclear Human Lens Fibers. Invest. Ophthalmol. Vis. Sci. 44, 1634–1642. https://doi.org/10.1167/iovs.02-0786

Ryazantsev, S.N., Poliansky, N.B., Chebotareva, N.A., Muranov, K.O., 2018. 3D structure of the native α-crystallin from bovine eye lens. Int. J. Biol. Macromol. 117, 1289–1298. https://doi.org/10.1016/j.ijbiomac.2018.06.004

Schreier, S., Polnaszek, C.F., Smith, I.C., 1978. Spin labels in membranes. Problems in practice. Biochim. Biophys. Acta 515, 395–436. https://doi.org/10.1016/0304-4157(78)90011-4

Schultz, K.M., Feix, J.B., Klug, C.S., 2013. Disruption of LptA oligomerization and affinity of the LptA-LptC interaction. Protein Sci. Publ. Protein Soc. 22, 1639–1645. https://doi.org/10.1002/pro.2369

Schultz, K.M., Lundquist, T.J., Klug, C.S., 2017. Lipopolysaccharide binding to the periplasmic protein LptA. Protein Sci. Publ. Protein Soc. 26, 1517–1523. https://doi.org/10.1002/pro.3177

Sean C. Semple, *, Arcadio Chonn, and, Cullis, P.R., 1996. Influence of Cholesterol on the Association of Plasma Proteins with Liposomes† [WWW Document]. https://doi.org/10.1021/bi950414i

Spector, A., 1984. The search for a solution to senile cataracts. Proctor lecture. Invest. Ophthalmol. Vis. Sci. 25, 130–146.

Srivastava, O.P., Srivastava, K., Silney, C., 1996. Levels of crystallin fragments and identification of their origin in water soluble high molecular weight (HMW) proteins of human lenses. Curr. Eye Res. 15, 511–520. https://doi.org/10.3109/02713689609000762

Stimmelmayr, R., Borchman, D., 2018. Lens Lipidomes among phocids and Odobenidae. Aquat. Mamm. 44, 496–508. https://doi.org/10.1578/AM.44.5.2018.506

Stottmann, R.W., Turbe-Doan, A., Tran, P., Kratz, L.E., Moran, J.L., Kelley, R.I., Beier, D.R., 2011. Cholesterol metabolism is required for intracellular hedgehog signal transduction in vivo. PLoS Genet. 7, e1002224. https://doi.org/10.1371/journal.pgen.1002224

Subczynski, W.K., Felix, C.C., Klug, C.S., Hyde, J.S., 2005. Concentration by centrifugation for gas exchange EPR oximetry measurements with loop-gap resonators. J. Magn. Reson. San Diego Calif 1997 176, 244–248. https://doi.org/10.1016/j.jmr.2005.06.011

Subczynski, W.K., Mainali, L., Raguz, M., O'Brien, W.J., 2017a. Organization of Lipids in Fiber-Cell Plasma Membranes of the Eye Lens. Exp. Eye Res. 156, 79–86. https://doi.org/10.1016/j.exer.2016.03.004

Subczynski, W.K., Pasenkiewicz-Gierula, M., Widomska, J., Mainali, L., Raguz, M., 2017b. High cholesterol/low cholesterol: Effects in biological membranes Review. Cell Biochem. Biophys. 75, 369–385. https://doi.org/10.1007/s12013-017-0792-7

Subczynski, W.K., Raguz, M., Widomska, J., Mainali, L., Konovalov, A., 2012. Functions of Cholesterol and the Cholesterol Bilayer Domain Specific to the Fiber-Cell Plasma Membrane of the Eye Lens. J. Membr. Biol. 245, 51–68. https://doi.org/10.1007/s00232-011-9412-4

Tang, D., Borchman, D., 1998. Temperature induced structural changes of beta-crystallin and sphingomyelin binding. Exp. Eye Res. 67, 113–118. https://doi.org/10.1006/exer.1998.0497

Tang, D., Borchman, D., Yappert, M.C., 1999. Alpha-crystallin/lens lipid interactions using resonance energy transfer. Ophthalmic Res. 31, 452–462. https://doi.org/10.1159/000055571

Tang, D., Borchman, D., Yappert, M.C., Cenedella, R.J., 1998. Influence of cholesterol on the interaction of alpha-crystallin with phospholipids. Exp. Eye Res. 66, 559–567. https://doi.org/10.1006/exer.1997.0467

Tate, M.W., Eikenberry, E.F., Turner, D.C., Shyamsunder, E., Gruner, S.M., 1991. Nonbilayer phases of membrane lipids. Chem. Phys. Lipids 57, 147–164. https://doi.org/10.1016/0009-3084(91)90073-K

Timsina, R., Khadka, N.K., Maldonado, D., Mainali, L., 2021. Interaction of alpha-crystallin with four major phospholipids of eye lens membranes. Exp. Eye Res. 202, 108337. https://doi.org/10.1016/j.exer.2020.108337

Truscott, R.J., 2000. Age-related nuclear cataract: a lens transport problem. Ophthalmic Res. 32, 185–194. https://doi.org/10.1159/000055612

Truscott, R.J.W., 2005. Age-related nuclear cataract-oxidation is the key. Exp. Eye Res. 80, 709–725. https://doi.org/10.1016/j.exer.2004.12.007

Van den Oetelaar, P.J.M., Van Someren, P.F.H.M., Thomson, J.A., Siezen, R.J., Hoenders, H.J., 1990. A dynamic quaternary structure of bovine .alpha.-crystallin as indicated from intermolecular exchange of subunits. Biochemistry 29, 3488–3493. https://doi.org/10.1021/bi00466a010

Veatch, S.L., Keller, S.L., 2003. A Closer Look at the Canonical 'Raft Mixture' in Model Membrane Studies. Biophys. J. 84, 725–726.

Vemuri, R., Philipson, K.D., 1989. Influence of sterols and phospholipids on sarcolemmal and sarcoplasmic reticular cation transporters. J. Biol. Chem. 264, 8680–8685.

Widomska, J., Subczynski, W.K., 2019. Why Is Very High Cholesterol Content Beneficial for the Eye Lens but Negative for Other Organs? Nutrients 11, 1083. https://doi.org/10.3390/nu11051083

Yang, S.-T., Kreutzberger, A.J.B., Lee, J., Kiessling, V., Tamm, L.K., 2016. The Role of Cholesterol in Membrane Fusion. Chem. Phys. Lipids 199, 136–143. https://doi.org/10.1016/j.chemphyslip.2016.05.003

Yappert, M.C., Rujoi, M., Borchman, D., Vorobyov, I., Estrada, R., 2003. Glycero- versus sphingo-phospholipids: correlations with human and non-human mammalian lens growth. Exp. Eye Res. 76, 725–734. https://doi.org/10.1016/S0014-4835(03)00051-4

Yue, H.-Y., Xu, J., 2015. Cholesterol regulates multiple forms of vesicle endocytosis at a mammalian central synapse. J. Neurochem. 134, 247–260. https://doi.org/10.1111/jnc.13129

Zelenka, P.S., 1984. Lens lipids. Curr. Eye Res. 3, 1337–1359. https://doi.org/10.3109/02713688409007421

Zhu, X., Gaus, K., Lu, Y., Magenau, A., Truscott, R.J.W., Mitchell, T.W., 2010. α- and β-Crystallins Modulate the Head Group Order of Human Lens Membranes during Aging. Invest. Ophthalmol. Vis. Sci. 51, 5162–5167. https://doi.org/10.1167/iovs.09-4947

Figure Captions

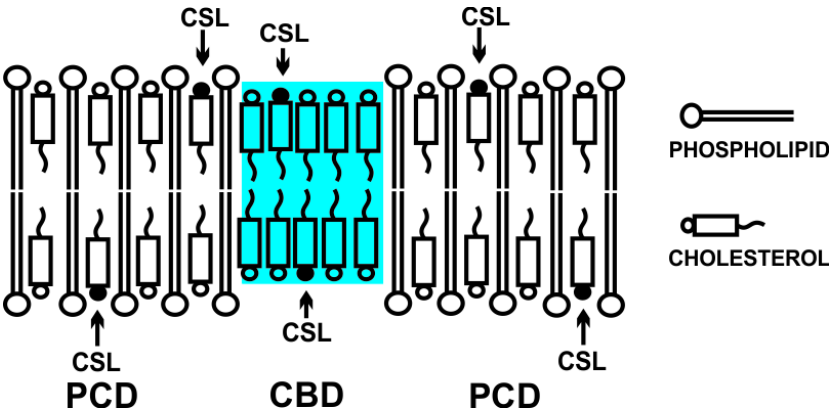

Fig. 1. Schematic drawing showing the distribution and approximate locations of cholesterol analog cholestane spin-label (CSL) within the phospholipid cholesterol domain (PCD) and cholesterol bilayer domain (CBD) in the membrane. The black dots represent the nitroxide moieties of the CSL spin-labels. The blue highlighted region represents the CBD.

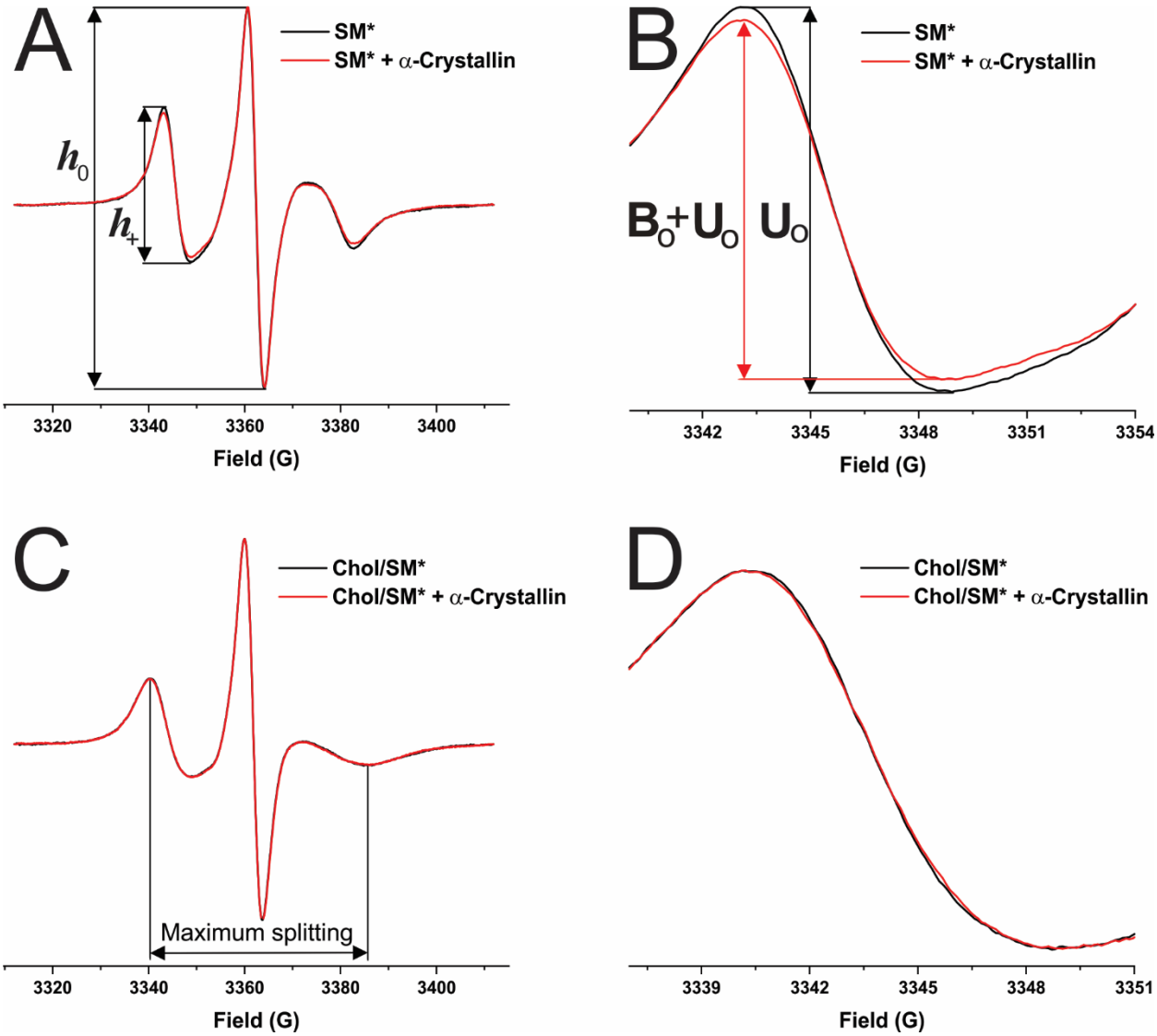

Fig. 2. (A) Representative EPR spectra of CSL in SM* membrane with Chol/SM* mixing ratio of 0 (no Chol) in the absence of α-crystallin (black) and 52.6 μM α-crystallin (red). (B) Zoomed low field line of the spectra in Fig. 2A. Fig. 2B shows that peak to peak intensity of the low field line of the EPR spectra decreased due to the binding of α-crystallin to the SM* membrane. (C) Representative EPR spectra of CSL in Chol/SM* membrane with Chol/SM* mixing ratio of 1.5 in the absence of α-crystallin (black) and 52.6 μM α-crystallin (red). Each EPR spectrum, as shown in (A) and (C), was normalized with respect to peak to peak intensity of the spectrum's central line. (D) Zoomed low field line of the spectra in Fig. 2C. Fig. 2D shows that peak to peak intensity of the low field line of the EPR spectra remained the same, representing no binding of α-crystallin to the Chol/SM* membrane with Chol/SM* mixing ratio of 1.5 (Chol inhibits the binding). The concentration of lipids (PL plus Chol) was maintained at 9.4 mM, and the concentration of α-crystallin was varied from 0 to 52.6 μM. All the samples were incubated at 37 °C for 16 h, and EPR measurements were taken at 37 °C. As shown in Fig. 2A, the ratio of peak to peak intensity of low field line (h_+) and the central line (h_0) of EPR spectra was used to calculate the mobility parameter (h_+/h_0) of the membranes. As shown in Fig. 2B, peak to peak intensities of low field EPR line of unbound (U_0) and unbound plus bound (U_0 +B_0) contributions were used to calculate the % CSL spin-labels affected (equation (1)) by α-crystallin binding, which then was used to calculate the K_a of α-crystallin to membranes (equation (4)). As shown in Fig. 2C, the horizontal distance between the low field and high field lines in the EPR spectra was used to calculate the maximum splitting.

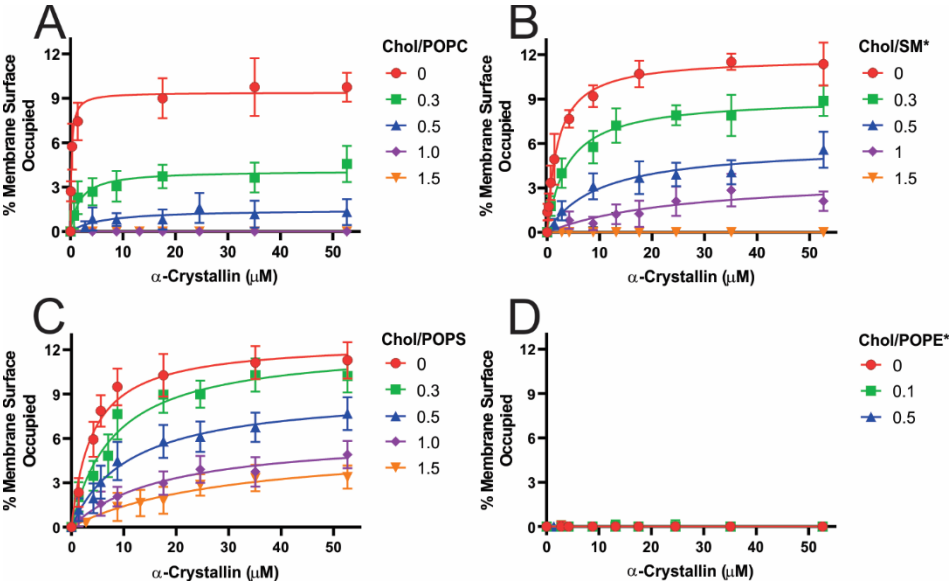

Fig. 3. (A), (B), (C), and (D) The percentage of membrane surface occupied (MSO) plotted as a function of α-crystallin concentration for the Chol/POPC, Chol/SM*, Chol/POPS, and Chol/POPE* membranes, respectively. For the Chol/POPC, Chol/SM*, and Chol/POPS membranes, the Chol/PL mixing ratios used were 0, 0.3, 0.5, 1.0, and 1.5. For the Chol/POPE* membrane, the Chol/POPE* mixing ratios used were 0, 0.1, and 0.5. The data for the POPC membrane at Chol/POPC mixing ratio of 0 and the POPS membrane at Chol/POPS mixing ratio of 0 were taken from our recent studies (Mainali et al., 2021) and (Timsina et al., 2021), respectively. The concentration of lipids (PL plus Chol) was maintained at 9.4 mM, and the concentration of α-crystallin was varied from 0 to 52.6 μM. The mixed α-crystallin and membranes samples were incubated at 37 °C for 16 h. Equation (2) was used to calculate the MSO. The data points in (A), (B), and (C) were fitted with a one-site ligand binding model (equation (3)) in GraphPad Prism (San Diego, CA) to estimate the K_a. The error bars were calculated from the average of three independent experiments. For the Chol/POPC, Chol/SM*, and Chol/POPS membrane, the MSO decreased with an increase in the Chol concentration, representing that Chol and CBDs inhibit the α-crystallin binding to these membranes. For the Chol/POPE* membranes at Chol/POPE* mixing ratios 0, 0.1, and 1.5, the MSO was zero for all concentrations of α-crystallin. It represents that there was no binding of α-crystallin to the Chol/POPE* membranes.

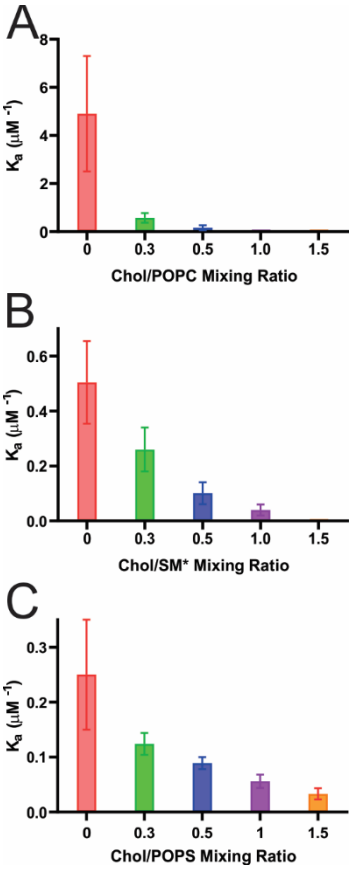

Fig. 4. (A), (B), and (C) The K_a for the Chol/POPC, Chol/SM*, and Chol/POPS membranes obtained by fitting the data points in Fig. 3A, B, and C, respectively, using a one-site ligand binding model (equation (3)). The data for the POPC membrane at Chol/POPC mixing ratio of 0 and the POPS membrane at Chol/POPS mixing ratio of 0 were taken from our recent studies (Mainali et al., 2021) and (Timsina et al., 2021), respectively. The concentration of lipids (PL plus Chol) was maintained at 9.4 mM, and the concentration of α-crystallin was varied from 0 to 52.6 μM. The mixed α-crystallin and membranes samples were incubated at 37 °C for 16 h. The EPR measurements were taken at 37 °C. The error bars were obtained from the three independent experiments. Since the K_a values were zero for the Chol/POPE* membranes (See MSO = 0 in Fig. 3D), no bar charts were shown for the Chol/POPE* membranes.

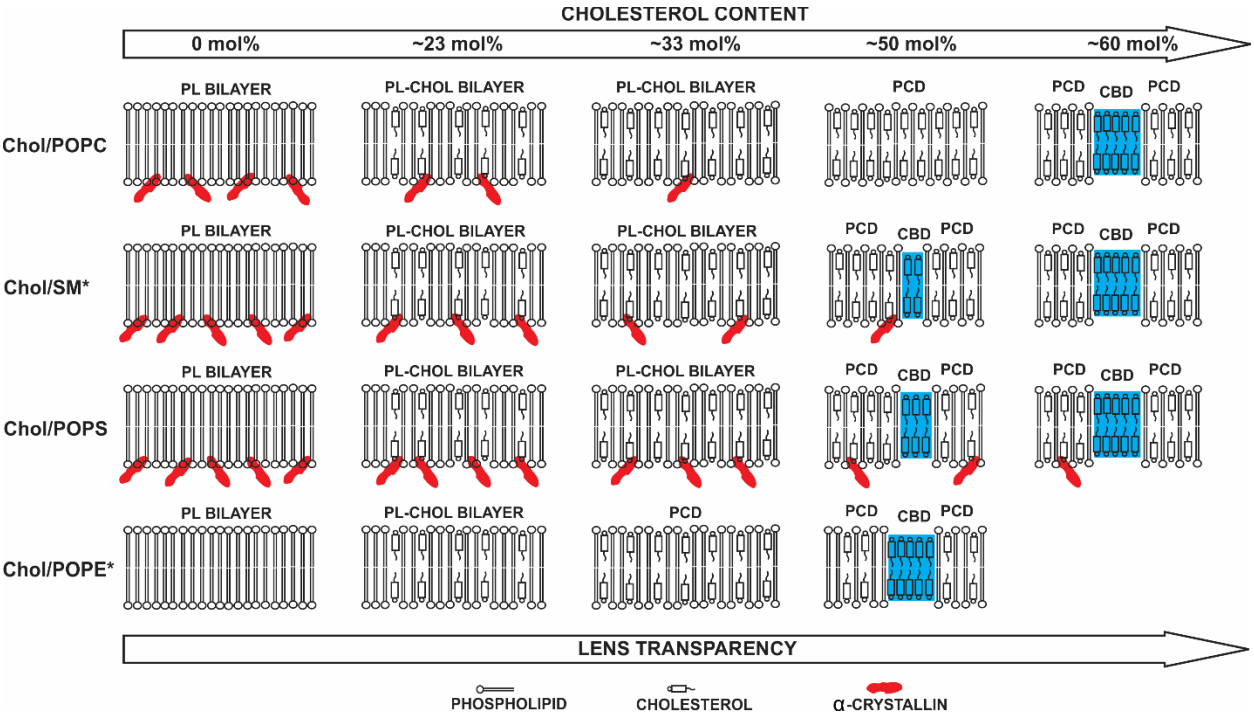

Fig. 5. Schematic drawing showing that the binding of α-crystallin to the Chol/PL (i.e., Chol/POPC, Chol/SM*, Chol/POPS, and Chol/POPE*) membranes with an increase in Chol content. With an increase in Chol content, membrane saturates with Chol and phospholipid cholesterol domain (PCD) forms. With further increase in Chol content, cholesterol bilayer domains (CBDs) form within the PCD. As shown in the blue highlighted regions, CBDs start to form at 50, 48, 46, and 33 mol% Chol in the PC, SM, PS, and PE membranes, respectively (Mainali et al., 2020). There was complete inhibition of α-crystallin binding to the Chol/POPC and Chol/SM* membranes at 50 mol% Chol (before CBDs' formation) and 60 mol% Chol (after CBDs formation), respectively. The binding of α-crystallin to the Chol/POPS membrane was not completely inhibited even at 60 mol% Chol (after CBDs' formation). There was no binding of α-crystallin to the Chol/POPE* membrane, even at 0 mol% Chol. We presented data for the Chol/POPE* membrane for 0, 9, and 33 mol% Chol only. Fig. 5 shows the schematic drawing representing the decrease in the amount of α-crystallin binding to the Chol/PL membranes with an increase in the Chol content in the membranes. The real size of the α-crystallin oligomer, represented by the red color in Fig. 5, is much larger than indicated in the schematic drawing. Due to the hydrophobic nature of the α-crystallin binding to the membrane, we think that only hydrophobic regions exposed on the surface of α-crystallin oligomer likely penetrate into the membrane reaching the hydrophobic region of the membrane. Previously, it was reported that denatured α-crystallin binds deep into the membrane (Borchman and Yappert, 2010; Cobb and Petrash, 2002b; Tang et al., 1999). The decrease in α-crystallin binding to the membranes implies a decrease in light scattering or increased lens transparency.

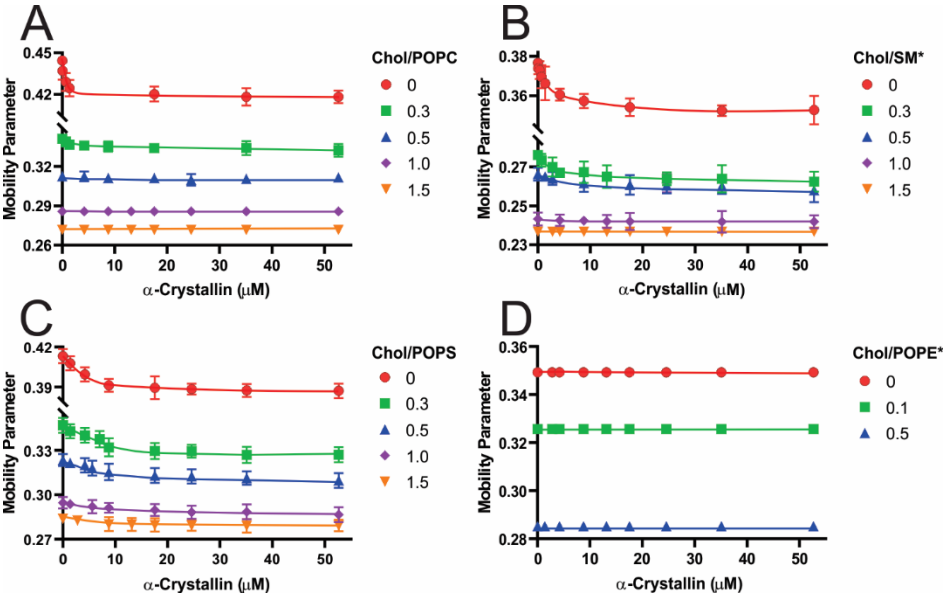

Fig. 6. The mobility parameter (h_+/h_0) profiles for Chol/PL membranes at different mixing ratios plotted as a function of α-crystallin concentration. (A), (B), and (C) include mobility parameter profiles for Chol/POPC, Chol/SM*, and Chol/POPS membranes, respectively, at mixing ratios 0, 0.3, 0.5, 1.0, and 1.5. (D) includes mobility parameter profiles for Chol/POPE* membrane at mixing ratios 0, 0.1, and 0.5. The data for the POPC membrane at Chol/POPC mixing ratio of 0 and the POPS membrane at the Chol/POPS mixing ratio of 0 were taken from our previous studies (Mainali et al., 2021) and (Timsina et al., 2021), respectively. The error bars were estimated from the average of three independent experiments. The concentration of lipids (PL plus Chol) was maintained at 9.4 mM, and the concentration of α-crystallin was varied from 0 to 52.6 μM. The samples were incubated at 37 ˚C for 16 h before taking EPR measurements at 37 ˚C. The mobility parameter was calculated using the method explained in section 2.6.

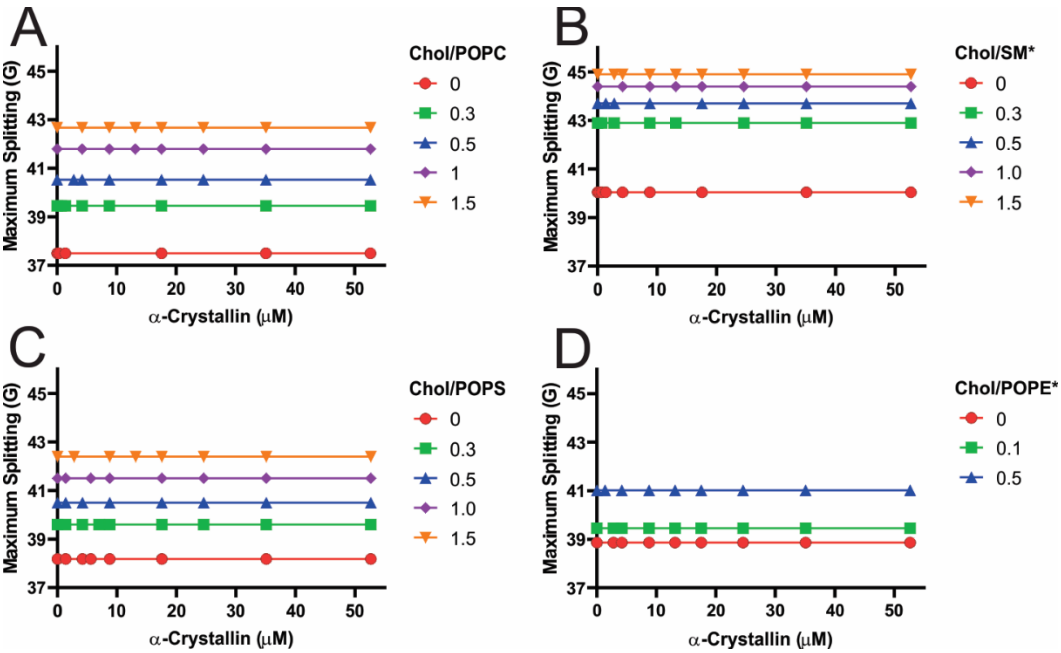

Fig. 7. The maximum splitting profiles for the Chol/PL membranes at different mixings ratios plotted as s function of α-crystallin concentration. (A), (B), and (C) include maximum splitting profiles for Chol/POPC, Chol/SM*, and Chol/POPS membranes, respectively, at mixing ratios 0, 0.3, 0.5, 1.0, and 1.5. (D) includes maximum splitting profiles for Chol/POPE* membrane at mixing ratios 0, 0.1, and 0.5. The data for the POPC membrane at the Chol/POPC mixing ratio of 0 and the POPS membrane at the Chol/POPS mixing ratio 0 were taken from our previous studies (Mainali et al., 2021) and (Timsina et al., 2021), respectively. The error bars were estimated from the average of three independent experiments. The error bars are not visible in the figure because the error bars are very small compared to the large range of maximum splitting plotted in the y-axis. The concentration of lipids (PL plus Chol) was maintained at 9.4 mM, and the concentration of α-crystallin was varied from 0 to 52.6 μM. The samples were incubated at 37 ˚C for 16 h before taking EPR measurements at 37 ˚C. The maximum splitting was calculated using the method explained in section 2.6.